DYNAMIC LOAD MODELING IN POWER SYSTEM ANALYSIS

by

Joseph Roger Gracia

Thesis submitted to the Graduate Faculty of the Virginia Polytechnic Institute and State University in partial fulfillment of the requirements for the degree of

MASTER OF SCIENCE

in

Electrical Engineering

APPROVED:

L. L. Grigsby

Dr. L. L. Grigsby, Chairman

N. A. Demerdash

Dr. N. A. Demerdash

Lee W. Johnson

Dr. Lee W. Johnson

August, 1977

Blacksburg, Virginia

ACKNOWLEDGEMENTS

The author wishes to express his thanks to Dr. L. L. Grigsby for serving as chairman of his graduate committee and to Dr. L. W. Johnson and Dr. N. A. Demerdash for serving as members of the committee. Special thanks are due to Dr. Grigsby for his guidance and encouragement throughout this investigation.

Thanks are also due to Cheryl West for doing an excellent job of typing this thesis and to the Energy Research Group for their financial support.

The help of Mr. D. T. Rizy, Mr. E. C. Gibson and other fellow graduate students is deeply appreciated as is the help of Mr. M. R. Shah in the formulation of the induction motor load model.

The author wishes to express special thanks to his wife Karen for her infinite patience, understanding and encouragement during this year in graduate school.

Last, but certainly not least, the author wishes to express sincere appreciation to his parents for their support, both moral and otherwise, and for being an unending source of inspiration throughout his lifetime.

TABLE OF CONTENTS

LIST OF FIGURES

LIST OF FIGURES, cont.:

LIST OF TABLES

1.0 INTRODUCTION

1.1 Background

Transient stability has long been of importance in the study of electric power systems, especially when generating stations are located far from the major load centers which they serve.

The ability of a power system to remain stable during any given disturbance is a function of many variables, the most obvious of which include:

1. the nature of the disturbance, its location and its duration;
2. the size and topology of the system under study;
3. the strength of ties with neighboring power systems.

Some factors which are not as obvious, yet affect the ability of any given power system to remain stable are:

4. the time of day at which the fault occurs;
5. the season of the year at which the fault occurs;
6. the particular types of customers the utility services, e.g. industrial, residential, agricultural, commercial.

To date, a great amount of research has been done in modeling the first group of variables, namely, the system itself, including a high degree of modeling of the generator, the fault and the effect of ties with neighboring systems. The second group of variables are not as easily modeled as the first group. These variables describe the types of loads which draw power from the different buses in the system. The wide variability among load types, the difficulty involved in collecting and classifying data on these loads, and the computational time and effort involved in their modeling (especially in the days of the net-

work analyzer) gave rise to three crude load models prevalent today: constant impedance, constant current and constant megavoltampere (MVA) (Fig. 1.1.1).

1.2 Classical Load Types

Load centers have historically been modeled, in the analysis of power system stability, as being composed of one or a combination of the following (Fig. 1.1.1):

1. Constant Impedance
2. Constant Current
3. Constant MVA

The complex power drawn by constant impedance loads is proportional to the square of the voltage, given that the system frequency remains at nominal value. Constant frequency will be assumed throughout this study. These types of loads have a damping effect on the system under study. This is due to the fact that most disturbances that will be encountered have the net effect of reducing the magnitude of the voltages throughout the system, especially near the fault. When these voltages dip, the currents drawn by the constant impedance loads dip accordingly. Most utility companies model their loads as constant impedance loads when studying the effect of a large-scale disturbance.

Constant current loads draw prefault current independent of the bus voltage. The most common combination of classical loads in studying large-scale disturbances is a constant current and constant impedance combination.

Few loads behave as the constant-MVA model does, especially when

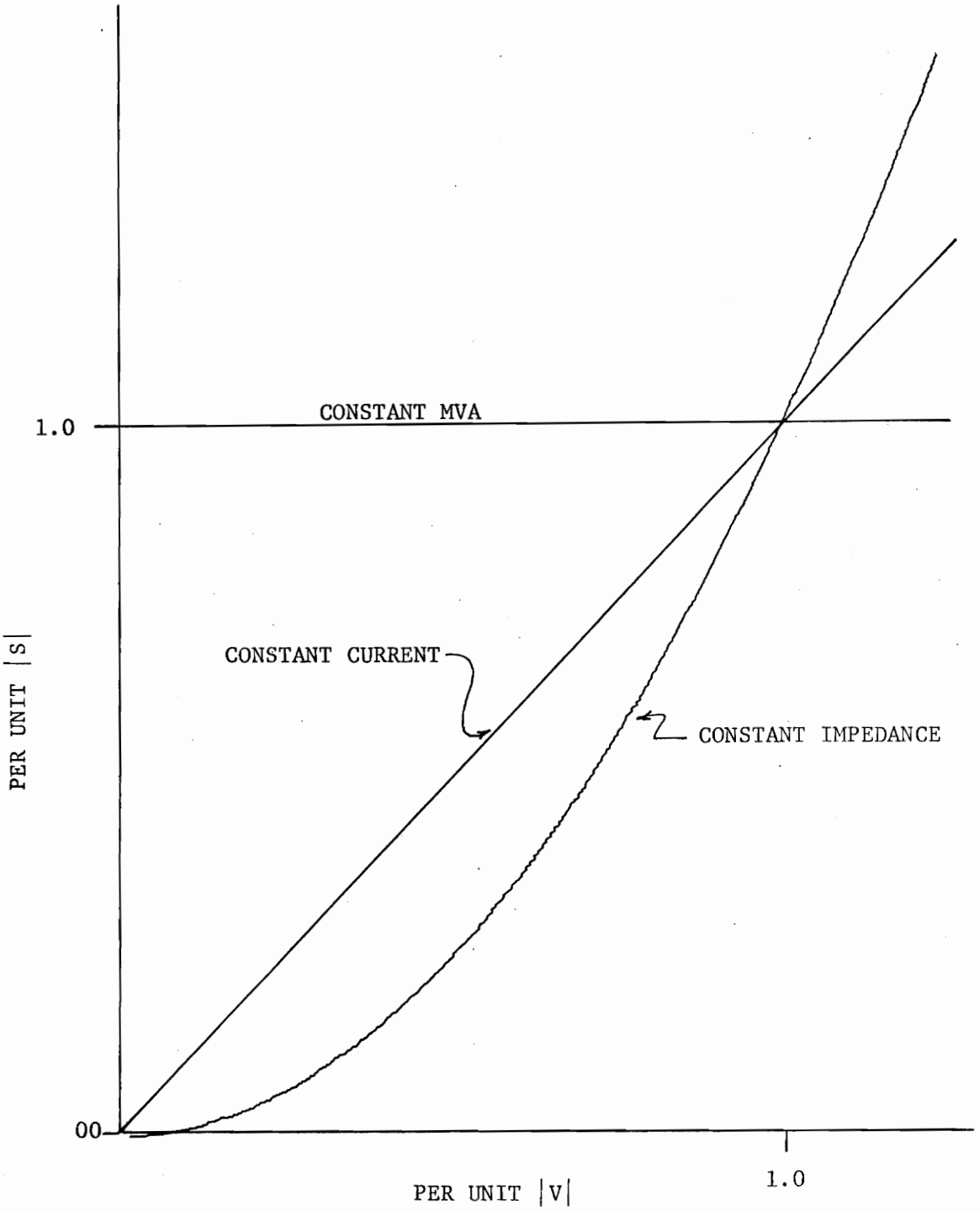

Fig. 1.1.1 - |S| - |V| Characteristics of Classical Load Models

the voltage dips very low. For most system topologies, this is the most severe model for a load, since as the voltage dips, the current increases. During a severe disturbance the currents can become quite large. Under small-scale voltage oscillations, induction motor loads behave nearly like constant-MVA loads. This justifies using such a severe load model since, with few exceptions, industrial loads are composed mainly of induction motors.

1.3 Drawbacks of Classical Load Types

The particulars describing load centers in power systems vary widely from one load center to another or even from one season of the year to another. One load center may consist of a manufacturing facility composed mainly of induction machines, such as an automobile assembly plant. Another load center may consist primarily of electric furnaces, such as are used in the mining and production of phosphorus. Residential loads may be primarily resistive in the winter, due to electric heating, cooking and water heaters. Yet, in the summer, residential loads may become significantly more reactive due to the effect of air conditioning.

Clearly, none of these situations can be adequately modeled as either constant impedance, constant current or constant MVA. Even though modeling the loads as a combination of these three is an improvement, it is still not totally satisfactory. An obvious drawback of any of these models is the fact that all loads are treated as static (inertialess) when, in reality, dynamic loads comprise a significant portion of the total power delivered by a utility.

These factors provide an impetus for research which will attempt to:

1. model inertialess and near inertialess loads more accurately than the classical load models;
2. account for the dynamics of prevalent non-static loads, i.e. induction motors;
3. ascertain whether refining the load model increases the accuracy obtained in a transient stability study to a high enough degree to make the extra computational effort worthwhile.

This research is presented herein. The question of the effect of frequency deviation is beyond the scope of this thesis.

2.0 MATHEMATICAL MODELS AND METHODS OF SOLUTION

2.1 Classical Load Models

Specific parameters describing power system loads under transient conditions are difficult, if not impossible, to obtain. Thus a need exists to model a load, in toto or in part, by one of the classical load models, namely constant impedance, constant current, or constant MVA.

When the load center being modeled is assumed to have constant-impedance characteristics, the equivalent load admittance at the ith bus ($\bar{Y}_{di}$) is computed from the complex power demand and the prefault bus voltage as follows:

Let $\bar{S}_{di}$ = total load power at bus i in per unit

$$= P_{di} + jQ_{di} \qquad (2.1.1)$$

and $\bar{V}_i$ = complex voltage at bus i.

Then, the equivalent shunt admittance to ground which will draw the given prefault load power at prefault voltage is given by

$$\bar{Y}_{di} = (\bar{S}^{\circ}_{di})^*/|V^{\circ}_i|^2$$

where the superscript "o" indicates the prefault value of the variable (Fig. 2.1.1-b).

Once this admittance is computed, it is added to the ith diagonal element of the bus impedance matrix ($\bar{Y}_{bus}$) where it remains (constant) throughout the solution time.

The active and reactive powers at a constant-impedance load bus vary as the square of the bus voltage magnitude, making this a fairly accurate representation of a load comprised mainly of industrial elec-

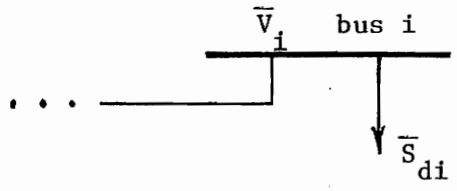

a. Steady State Load

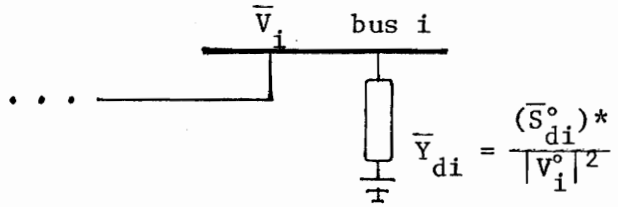

b. Constant Impedance

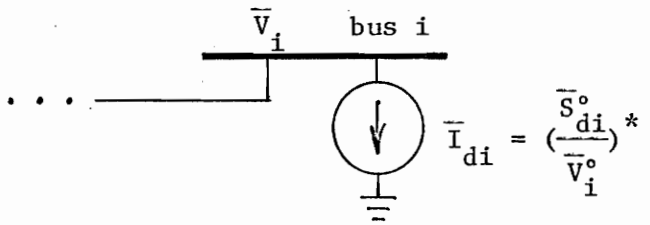

c. Constant Current

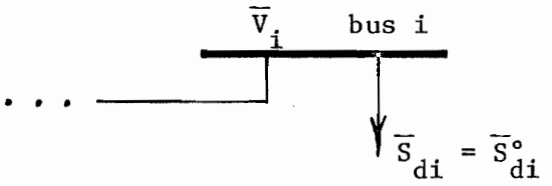

d. Constant MVA

Fig. 2.1.1 Classical Load Models

tric furnaces or a residential area in the wintertime.

When the complex power at a load center exhibits a linear or nearly-linear relationship with the complex voltage, at least for some voltage range, the model which will most closely represent it will be the constant current model (Fig. 1.1.1, Fig. 2.1.1-c). The current which draws the specified prefault complex power at prefault bus voltage ($\bar{I}_{di}$) is given by:

$$\bar{I}_{di} = (\bar{S}^{\circ}_{di}/\bar{V}^{\circ}_{i})^{*} \qquad (2.1.3)$$

The load current computed by Eq. (2.1.3) is kept constant throughout the solution time. Section 2.5 describes the role of $\bar{I}_{di}$ in the solution procedure.

The last of the classical loads is the constant MVA model. The magnitude of the load power is assumed to remain constant at the specified prefault level regardless of the voltage at the load bus. The model is simply given as follows (Fig. 2.1.1-d):

$$\bar{S}_{di} = \bar{S}^{\circ}_{di} \qquad (2.1.4)$$

This type of model causes the load currents to become unwieldingly large at load buses in the vicinity of a short circuit due to the voltage drop associated with that type of disturbance. Since most loads do not behave in this manner, this model is seldom used.

2.2 Polynomial Approximation of Load-Voltage Characteristics

In the previous section, the loads in question were modeled in a way that decoupled the load characteristic from the bus voltage. A more accurate model would represent the loads as a function of both voltage and frequency. Since the frequency is assumed to remain constant

throughout the solution time in this study, the load curves reduce to a function of voltage only.

At each load bus, there will be a mixture of devices (load types) drawing power from the bus, e.g. induction motors and fluorescent lights at an industrial site. The total load power drawn at a bus will be, by conservation of power, the sum of the complex powers drawn by each individual load type at the given bus. Specifically:

Let $\bar{S}_{ij}$ = complex power being drawn by load type j at bus i

$$= P_{ij} + jQ_{ij} \qquad (2.2.1)$$

Then $$\bar{S}_{di} = \sum_{j=1}^{m} \bar{S}_{ij} \qquad (2.2.2)$$

where m = number of different load types being served by the utility company

There are two basic philosophies of expressing load curves as a function of the bus voltage:

1. express the real and reactive powers as proportional to a possibly non-integer power of the voltage magnitude;
2. express the real and reactive powers as proportional to a polynomial expansion of the voltage magnitude.

The real and reactive powers described in case 1 can be represented as follows:

$$P_{ij} = c_{ij}|V_i|^{p_j} \qquad (2.2.3\text{-a})$$

$$Q_{ij} = d_{ij}|V_i|^{q_j} \qquad (2.2.3\text{-b})$$

where p_j = an exponent (possibly non-integer) describing the P-V characteristic,

q_j = an exponent (possibly non-integer) describing the Q-V

characteristic, and

c_{ij}, d_{ij} = constants of proportionality.

Limiting consideration to small changes in voltage, the real power drawn by load type j at bus i at the (k+1)th iteration can be approximated by the following truncated Taylor's series expansion:

$$P_{ij}^{(k+1)} = P_{ij}^{(k)} + \left.\frac{dP_{ij}}{d|V_i|}\right|_k \Delta|V_i|^{(k)} \qquad (2.2.4\text{-a})$$

where $P_{ij}^{(k+1)}$ = real power drawn by load type j at bus i at the (k+1)th iteration;

$\left.\frac{dP_{ij}}{d|V_i|}\right|_k$ = derivative of power with respect to voltage magnitude evaluated at the kth iteration; and

$$\Delta|V_i|^{(k)} = |V_i|^{(k+1)} - |V_i|^{(k)} \qquad (2.2.5)$$

= change in voltage magnitude at bus i at the kth iteration.

Similarly, for the reactive power:

$$Q_{ij}^{(k+1)} = Q_{ij}^{(k)} + \left.\frac{dQ_{ij}}{d|V_i|}\right|_k \Delta|V_i|^{(k)} \qquad (2.2.4\text{-b})$$

By expressing P_{ij} and Q_{ij} as proportional to a possibly non-integer power of the voltage magnitude (Eq. 2.2.3), the derivatives in Eqs. (2.2.4) become

$$\left.\frac{dP_{ij}}{d|V_i|}\right|_k = c_{ij}p_j(|V_i|^{(k)})^{p_j-1} \qquad (2.2.6\text{-a})$$

and

$$\left.\frac{dQ_{ij}}{d|V_i|}\right|_k = d_{ij}q_j(|V_i|^{(k)})^{q_j-1} \qquad (2.2.6\text{-b})$$

Thus, eqs. (2.2.4) yield an iterative relationship for the powers.

This model, although satisfactory in the analysis of small-scale perturbations around an operating point, loses validity during major disturbances when voltages are likely to dip considerably.

The second philosophy, where the active and reactive powers are expressed as a polynomial in voltage magnitude, represents a more accurate model when wide voltage deviations are considered.

It can be shown [6, 9, 14, 15] that, given k data points (x_1, y_1), (x_2, y_2), ..., (x_k, y_k), there is one and only one polynomial

$$f(x) = a_o + a_1 x + a_2 x^2 + \ldots + a_{k-1} x^{k-1} \qquad (2.2.7)$$

such that

$$f(x_i) = y_i \qquad (2.2.8)$$

This polynomial is known by many names, the most prevalent being the interpolating polynomial.

Given k data points, however, a kth-order interpolating polynomial will, in general, not be desirable. This is due to the fact that the values used as data points are not absolutely correct due to a certain degree of experimental error associated with each point. Representing this data in an exact manner, then, would be meaningless since the data itself is not exact. What is needed, then, is a model that will "smooth out" the data points.

This leads to a least-squares type approximation, where the data points are approximated by an nth-order polynomial ($n < k - 1$)

$$f(x) = a_o + a_1 x + a_2 x^2 + \ldots + a_n x^n, \quad n < k - 1 \qquad (2.2.9)$$

For the polynomial approximation in eq. (2.2.9) of the k data points, the following over-determined linear system must be solved:

$$\begin{bmatrix} 1 & x_1 & x_1^2 & \cdots & x_1^n \\ 1 & x_2 & x_2^2 & \cdots & x_2^n \\ 1 & x_3 & x_3^2 & \cdots & x_3^n \\ 1 & x_4 & x_4^2 & \cdots & x_4^n \\ 1 & x_5 & x_5^2 & \cdots & x_5^n \\ 1 & x_6 & x_6^2 & \cdots & x_6^n \\ \vdots & \vdots & \vdots & & \vdots \\ 1 & x_k & x_k^2 & \cdots & x_k^n \end{bmatrix}_{kxn} \begin{bmatrix} a_o \\ a_1 \\ \vdots \\ a_n \end{bmatrix}_{nx1} = \begin{bmatrix} y_1 \\ y_2 \\ y_3 \\ y_4 \\ y_5 \\ y_6 \\ \vdots \\ y_k \end{bmatrix}_{kx1} \tag{2.2.10}$$

or, in matrix notation,

$$\underline{\underline{x}}\underline{a} = \underline{y} \tag{2.2.11}$$

Since a unique vector $\underline{a}$ which satisfies this set of constraints does not exist, one must find an n-vector $\underline{a}^*$ such that

$$\| \underline{y} - \underline{\underline{x}}\underline{a}^* \| \leq \| \underline{y} - \underline{\underline{x}}\underline{a} \| \tag{2.2.12}$$

for all n-vectors $\underline{a}$.

That is, to find a "solution" $\underline{a}^*$ which minimizes the sum of the squares of errors between the ordinates of the experimental data points and the value calculated by the nth order polynomial approximation. The norm of any vector $\underline{z}$ is given by

$$\| \underline{z} \| = \sqrt{|z_1|^2 + \ldots + |z_n|^2} \tag{2.2.13}$$

In symbols, let

$$\hat{y}_i = a_o + a_1 x_i + a_2 x_i^2 + \ldots + a_n x_i^n = f(x_i), \tag{2.2.14}$$

y_i = experimentally obtained ordinate corresponding to x_i, and

$$e_i = y_i - \hat{y}_i. \tag{2.2.15}$$

The optimum solution $\underset{\sim}{a}^*$ must minimize

$$\sum_{j=1}^{k} e_i^2 = \sum_{j=1}^{k} (y_i - \hat{y}_i)^2 = \| \underset{\sim}{y} - \underset{\sim}{x}\underset{\sim}{a}\|^2 \tag{2.2.16}$$

Thus, this optimum solution $\underset{\sim}{a}^*$ for the polynomial coefficients a_o, a_1, ..., a_n ($n<k-1$, k data points) is the best in the least-squares sense. It can be proved [6,14,15] that this $\underset{\sim}{a}^*$ can be obtained by solving the system

$$\underset{\sim}{x}^T\underset{\sim}{x}\underset{\sim}{a} = \underset{\sim}{x}^T\underset{\sim}{y} \tag{2.2.17}$$

or

$$\underset{\sim}{a}^* = (\underset{\sim}{x}^T\underset{\sim}{x})^{-1}\underset{\sim}{x}^T\underset{\sim}{y}. \tag{2.2.18}$$

The matrix $(\underset{\sim}{x}^T\underset{\sim}{x})^{-1}\underset{\sim}{x}^T$ is referred to as the pseudo-inverse of $\underset{\sim}{x}$. Clearly, if the system matrix $\underset{\sim}{x}$ is square, then

$$(\underset{\sim}{x}^T\underset{\sim}{x})^{-1}\underset{\sim}{x}^T = \underset{\sim}{x}^{-1}(\underset{\sim}{x}^T)^{-1}\underset{\sim}{x}^T = \underset{\sim}{x}^{-1} \tag{2.2.19}$$

that is, the pseudo-inverse reduces to the true inverse of the square matrix (assuming $\underset{\sim}{x}$ is non-singular).

The loads in this study were represented as a fourth-order polynomial in V; that is, for each different load type, there are two fourth-order polynomials in V representing the P-V and Q-V characteristics of the load in question. The real power drawn by load type j at bus i is given by:

$$P_{ij} = c_{ij} f_j(|V_i|) \tag{2.2.20}$$

$$= c_{ij}[(a_o)_j + (a_1)_j|V_i| + (a_2)_j|V_i|^2 + (a_3)_j|V_i|^3 + (a_4)_j|V_i|^4] \tag{2.2.21}$$

where c_{ij} is a constant that normalizes the function value at prefault voltage to prefault power. The constant c_{ij} is calculated immediately after performing the prefault loadflow as follows:

$$c_{ij} = \frac{P^{\circ}_{ij}}{f_j(|V^{\circ}_i|)} \tag{2.2.22}$$

where, as mentioned previously, the superscript "o" denotes prefault values.

Similarly, for the reactive power at bus i,

$$Q_{ij} = d_{ij} g_j(|V_i|) \tag{2.2.23}$$

$$= d_{ij}[(b_o)_j + (b_1)_j|V_i| + (b_2)_j|V_i|^2 + (b_3)_j|V_i|^3 + (b_4)_j|V_i|^4] \tag{2.2.24}$$

where

$$d_{ij} = \frac{Q^{\circ}_{ij}}{g_j(|V^{\circ}_i|)} \tag{2.2.25}$$

At this juncture, a recapitulation of the load models used in analyzing the effects of large-scale disturbances is in order. The classical constant impedance, constant current, and constant MVA models, given by eqs. (2.1.2), (2.1.3) and (2.1.4), respectively, are repeated below:

$$\bar{Y}_{di} = (\bar{S}^{\circ}_{di})^*/|V^{\circ}_i|^2 \tag{2.1.2}$$

$$\bar{I}_{di} = (\bar{S}^{\circ}_{di}/\bar{V}^{\circ}_i)^* \tag{2.1.3}$$

$$\bar{S}_{di} = \bar{S}^{\circ}_{di} \tag{2.1.4}$$

Polynomial approximations to load-voltage characteristics of a specific load type j are given by:

$$P_{ij} = c_{ij} f_j(|V_i|) \qquad (2.2.20)$$

$$Q_{ij} = d_{ij} g_j(|V_i|) \qquad (2.2.23)$$

where c_{ij} and d_{ij} are the appropriate constants of proportionality.

The first three models are useful when specific data on a load center is, for one reason or another, unavailable. The last one is useful when load-voltage characteristic data for certain load types is known. In all these models, however, the complex power drawn is represented, at best, as a function of the bus voltage at the present time only. This limits the types of loads modeled to being either static or quasi-static. Since a great part of the energy supplied by a utility company powers dynamic loads, namely induction motors, another load representation which models the dynamics of this type of machine will be developed and used.

2.3 Induction Motor Loads

Induction motor loads represent a considerable portion of the total load served by an electric power utility company, especially in a heavily industrialized area. Since the effects of the induction motor transients on the generator swing curves will be studied, a dynamic model which accounts for both electrical and mechanical transients will be used. In the model presented herein, the quantities involved are expressed in per-unit, as are all quantities in this study.

Modeling each individual induction machine in an industrial load center is a formidable task, especially when many load centers are involved. For the purposes of this study, all machines will be combined and represented as a single equivalent induction motor, repre-

sentable in the steady state by Fig. (2.3.1).

Fig. (2.3.2) depicts the transient model of the induction machine [7,19]. The differential equation describing the rate of change of the induction motor equivalent emf $\bar{E}'$ behind the transient impedance at bus i is given by:

$$\frac{d\bar{E}'_i}{dt} = -j\omega\sigma_i\bar{E}'_i - \frac{1}{(T_o)_i}\{\bar{E}'_i - j(X_i - X'_i)(\bar{I}_m)_i\} \qquad (2.3.1)$$

where $j = \sqrt{-1}$,

ω = synchronous angular speed,

σ_i = slip of machine at bus i,

$(T_o)_i$ = rotor open-circuit time constant of machine at bus i,

X_i = open circuit reactance of machine at bus i,

X'_i = blocked rotor reactance of machine at bus i,

$\bar{I}_{mi}$ = current drawn by equivalent machine at bus i.

When combined with the motor swing equation, both rotor electrical and mechanical transients are modeled. The dynamic model parameters can be computed from the steady-state equivalent circuit parameters as follows:

$$\sigma_i = \frac{\omega - \omega_{act,i}}{\omega} \qquad (2.3.2)$$

$$(T_o)_i = \frac{x_{ri} + x_{mi}}{\omega r_{ri}} \qquad (2.3.3)$$

$$X_i = x_{si} + x_{mi} \qquad (2.3.4)$$

$$X'_i = x_{si} + \frac{x_{mi}x_{ri}}{x_{mi} + x_{ri}} \qquad (2.3.5)$$

To simplify notation, the subscripts indicating the ith bus will be dropped. The development that follows holds true in general for any machine at any bus even though the subscript has been omitted. Rewriting

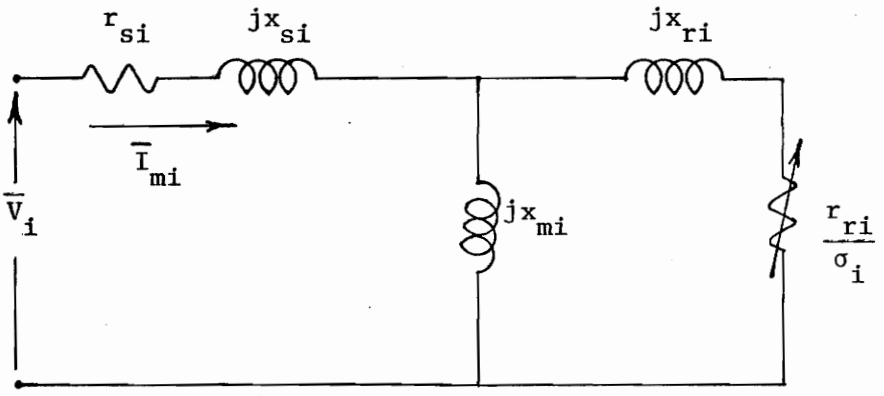

Fig. 2.3.1 Steady State Equivalent Circuit of Induction Motor at Bus i.

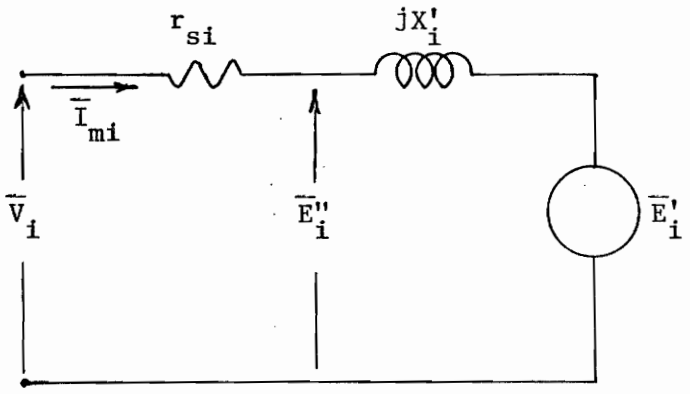

Fig. 2.3.2 Equivalent Circuit of Induction Machine at Bus i Under Transient Conditions

eq. (2.3.1) using the new convention yields the following:

$$\frac{d\bar{E}'}{dt} = -j\omega\sigma\bar{E}' - \frac{1}{T_o}\{\bar{E}' - j(X - X')\bar{I}_m\} \qquad (2.3.6)$$

But the motor current is given by

$$\bar{I}_m = \frac{\bar{E}'' - \bar{E}'}{jX'} \qquad (2.3.7)$$

where $\bar{E}''$ is the voltage between the stator resistance and the transient reactance (Fig. 2.3.2).

Substituting the expression obtained for the current into eq. (2.3.6) yields

$$\frac{d\bar{E}'}{dt} = -j\omega\sigma\bar{E}' - \frac{1}{T_o}\{\bar{E}' - j(X - X')\frac{(\bar{E}'' - \bar{E}')}{jX'}\} \qquad (2.3.8)$$

Suppose

$$\bar{E}' = a' + jb' \qquad (2.3.9)$$

$$\bar{E}'' = a'' + jb'' \qquad (2.3.10)$$

Then,

$$\frac{d\bar{E}'}{dt} = \frac{d}{dt}(a' + jb') = -j\omega\sigma(a' + jb') - \frac{(a' + jb')}{T_o} + \frac{1}{T_o}\left(\frac{X - X'}{X'}\right)((a'' - a') + j(b'' - b')) \qquad (2.3.11)$$

Separating real and imaginary parts and grouping terms gives the following pair of coupled differential equations:

$$\frac{da'}{dt} = a'\left[\frac{-1}{T_o} - \frac{1}{T_o}\left(\frac{X - X'}{X'}\right)\right] + b'[\omega\sigma] + \frac{a''}{T_o}\left(\frac{X - X'}{X'}\right) \qquad (2.3.12\text{-a})$$

$$\frac{db'}{dt} = a'[-\omega\sigma] + b'\left[\frac{-1}{T_o} - \frac{1}{T_o}\left(\frac{X - X'}{X'}\right)\right] + \frac{b''}{T_o}\left(\frac{X - X'}{X'}\right) \qquad (2.3.12\text{-b})$$

Recognizing that

$$\frac{-1}{T_o} - \frac{1}{T_o}\left(\frac{X - X'}{X'}\right) = \frac{-1}{T_o}\frac{X}{X'}, \tag{2.3.13}$$

the pair of differential equations (2.3.12) reduces to the following second-order system:

$$\begin{bmatrix} \dot{a}' \\ \dot{b}' \end{bmatrix} = \begin{bmatrix} \frac{-1}{T_o}\frac{X}{X'} & \omega\sigma \\ -\omega\sigma & \frac{-1}{T_o}\frac{X}{X'} \end{bmatrix} \begin{bmatrix} a' \\ b' \end{bmatrix} + \begin{bmatrix} \frac{a''}{T_o}\left(\frac{X - X'}{X'}\right) \\ \frac{b''}{T_o}\left(\frac{X - X'}{X'}\right) \end{bmatrix} \tag{2.3.14}$$

where the dot over a variable indicates time differentiation. The system of equations (2.3.14) is identical to the complex-valued equation (2.3.8) provided that

$$\frac{d\bar{E}'}{dt} = \dot{a}' + j\dot{b}' \tag{2.3.15}$$

Since the slip σ and the forcing function E' are not constant, eq. (2.3.14) represents a time-varying system. By limiting consideration to a small time increment Δt, σ and E' can be considered constant. Under these assumptions, at each iteration eq. (2.3.14) represents a time-invariant linear system in standard form

$$\dot{\underline{x}} = \underline{A}\underline{x} + \underline{B}\underline{u} \tag{2.3.16}$$

A closed-form solution can now be obtained, thereby achieving a considerable savings in computer time.

Taking the Laplace transform of both sides of eq. (2.3.14) (under the assumption that σ and E are constant during the solution interval) yields:

$$\begin{bmatrix} s & o \\ 0 & s \end{bmatrix} \begin{bmatrix} A' \\ B' \end{bmatrix} - \begin{bmatrix} A'(t_o) \\ B'(t_o) \end{bmatrix} = \begin{bmatrix} \frac{-1}{T_o}\frac{X}{X'} & \omega\sigma \\ -\omega\sigma & \frac{-1}{T_o}\frac{X}{X'} \end{bmatrix} \begin{bmatrix} A' \\ B' \end{bmatrix} + \frac{1}{s}\begin{bmatrix} \hat{a} \\ \hat{b} \end{bmatrix} \tag{2.3.17}$$

where capital letters indicate Laplace-transformed quantities and

$$\hat{a} = \frac{a''}{T_o}\left(\frac{X - X'}{X'}\right) \tag{2.3.18-a}$$

$$\hat{b} = \frac{b''}{T_o}\left(\frac{X - X'}{X'}\right) \tag{2.3.18-b}$$

Regrouping terms one obtains

$$\begin{bmatrix} A' \\ B' \end{bmatrix} = \begin{bmatrix} \left(s + \frac{1}{T_o}\frac{X}{X'}\right) & -\omega\sigma \\ \omega\sigma & \left(s + \frac{1}{T_o}\frac{X}{X'}\right) \end{bmatrix}^{-1} \left\{ \begin{bmatrix} A'(t_o) \\ B'(t_o) \end{bmatrix} + \frac{1}{s}\begin{bmatrix} \hat{a} \\ \hat{b} \end{bmatrix} \right\} \tag{2.3.19}$$

Performing the indicated inversion gives

$$\begin{bmatrix} A' \\ B' \end{bmatrix} = \frac{1}{\left(s + \frac{1}{T_o}\frac{X}{X'}\right)^2 + (\omega\sigma)^2} \begin{bmatrix} \left(s + \frac{1}{T_o}\frac{X}{X'}\right) & \omega\sigma \\ -\omega\sigma & \left(s + \frac{1}{T_o}\frac{X}{X'}\right) \end{bmatrix}$$

$$\left\{ \begin{bmatrix} A'(t_o) \\ B'(t_o) \end{bmatrix} + \frac{1}{s}\begin{bmatrix} \hat{a} \\ \hat{b} \end{bmatrix} \right\} \tag{2.3.20}$$

Inverse Laplace-transforming both sides of this equation yields the following:

$$\begin{bmatrix} a'(t) \\ b'(t) \end{bmatrix} = \underset{\sim}{\hat{\Phi}} \begin{bmatrix} a'(t_o) \\ b'(t_o) \end{bmatrix} + \underset{\sim}{\hat{\Theta}} \begin{bmatrix} \hat{a} \\ \hat{b} \end{bmatrix} \tag{2.3.21}$$

where

$$\underset{\sim}{\hat{\Phi}} = \begin{bmatrix} \exp\left(-\frac{1}{T_o}\frac{X}{X'}t\right)\cos\omega\sigma t & \exp\left(\frac{-1}{T_o}\frac{X}{X'}t\right)\sin\omega\sigma t \\ -\exp\left(-\frac{1}{T_o}\frac{X}{X'}t\right)\sin\omega\sigma t & \exp\left(\frac{-1}{T_o}\frac{X}{X'}t\right)\cos\omega\sigma t \end{bmatrix} \tag{2.3.22}$$

and

$$\hat{\underset{\sim}{\Theta}} = \frac{1}{\left(\frac{1}{T_o}\frac{X}{X'}\right)^2 + (\omega\sigma)^2}\begin{bmatrix} \{\exp(\frac{-1}{T_o}\frac{X}{X'}\,t)(\frac{-1}{T_o}\frac{X}{X'}\cos\omega\sigma t + \omega\sigma\sin\omega\sigma t) + \frac{1}{T_o}\frac{X}{X'}\} & \\ -\{\exp(\frac{-1}{T_o}\frac{X}{X'}\,t)(\frac{-1}{T_o}\frac{X}{X'}\sin\omega\sigma t - \omega\sigma\cos\omega\sigma t) + \omega\sigma\} & \end{bmatrix}$$

$$\begin{bmatrix} \{\exp(\frac{-1}{T_o}\frac{X}{X'}\,t)(\frac{-1}{T_o}\frac{X}{X'}\sin\omega\sigma t - \omega\sigma\cos\omega\sigma t) + \omega\sigma\} & \\ \{\exp(\frac{-1}{T_o}\frac{X}{X'}\,t)(\frac{-1}{T_o}\frac{X}{X'}\cos\omega\sigma t + \omega\sigma\sin\omega\sigma t) + \frac{1}{T_o}\frac{X}{X'}\} & \end{bmatrix} \qquad (2.3.23)$$

Since consideration is limited to small time increments, time is discretized in the following manner:

Let

$$t_o = n\Delta t \qquad (2.3.24)$$

$$= \text{time at the nth iteration,}$$

$$t = t_o + \Delta t \qquad (2.3.25)$$

$$= (n+1)\Delta t \qquad (2.3.26)$$

$$= \text{time at the (n+1)th iteration.}$$

Then the $\hat{\underset{\sim}{\Phi}}$ and $\hat{\underset{\sim}{\Theta}}$ matrices used to calculate the real and reactive portion of the transient emf $\bar{E}'$ at the (n+1)th iteration are given by

$$\hat{\underset{\sim}{\Phi}}(n) = \exp(\frac{-1}{T_o}\frac{X}{X'}\Delta t)\begin{bmatrix} \cos\omega\sigma\Delta t & \sin\omega\sigma\Delta t \\ -\sin\omega\sigma\Delta t & \cos\omega\sigma\Delta t \end{bmatrix} \qquad (2.3.27)$$

and

$$\hat{\underset{\sim}{\Theta}}(n) = \frac{1}{(\frac{1}{T_o}\frac{X}{X'})^2+(\omega\sigma)^2}\begin{bmatrix} \{\exp(\frac{-1}{T_o}\frac{X}{X'}\Delta t)(\frac{-1}{T_o}\frac{X}{X'}\cos\omega\sigma\Delta t + \omega\sigma\sin\omega\sigma\Delta t) + \frac{1}{T_o}\frac{X}{X'}\} \\ -\{\exp(\frac{-1}{T_o}\frac{X}{X'}\Delta t)(\frac{-1}{T_o}\frac{X}{X'}\sin\omega\sigma\Delta t - \omega\sigma\cos\omega\sigma\Delta t) + \omega\sigma\} \end{bmatrix}$$

$$\begin{bmatrix} \{\exp(\frac{-1}{T_o}\frac{X}{X'}\Delta t)(\frac{-1}{T_o}\frac{X}{X'}\sin\omega\sigma\Delta t - \omega\sigma\cos\omega\sigma\Delta t) + \omega\sigma\} \\ \{\exp(\frac{-1}{T_o}\frac{X}{X'}\Delta t)(\frac{-1}{T_o}\frac{X}{X'}\cos\omega\sigma\Delta t + \omega\sigma\sin\omega\sigma\Delta t) + \frac{1}{T_o}\frac{X}{X'}\} \end{bmatrix} \qquad (2.3.28)$$

These matrices must be calculated at each iteration. The iterative equation then becomes

$$\begin{bmatrix} a'(n+1) \\ b'(n+1) \end{bmatrix} = \hat{\underset{\sim}{\Phi}}(n)\begin{bmatrix} a'(n) \\ b'(n) \end{bmatrix} + \hat{\underset{\sim}{\Theta}}(n)\begin{bmatrix} \hat{a}(n) \\ \hat{b}(n) \end{bmatrix} \qquad (2.3.29)$$

To this point, only the dynamics of the transient emf E' have been discussed. Coupled to these are the mechanical dynamics of the machine.

The masses of rotating machines can be modeled as

$$\ddot{\delta} = -D\frac{\pi f}{H}\dot{\delta} + \frac{\pi f}{H}P_a \qquad (2.3.30)$$

where H = inertia constant,

D = damping constant,

$\pi \cong 3.14159265$,

f = synchronous frequency,

P_a = accelerating power.

Assuming the motors in question are undamped, that is, D = 0, equation (2.3.30) reduces to

$$\ddot{\delta} = \frac{\pi f}{H}(P_m - P_e) \qquad (2.3.31)$$

where the accelerating power has been defined as

$$P_a = P_m - P_e \tag{2.3.32}$$

and

P_m = mechanical load on motor

P_e = electrical torque-producing power in motor.

The slip is defined as:

$$\sigma = \frac{\omega - \omega_{act}}{\omega} \tag{2.3.33}$$

where

ω = synchronous angular velocity,

ω_{act} = actual angular velocity.

Since

$$\dot{\delta} = \omega - \omega_{act}, \tag{2.3.34}$$

the slip can be expressed as

$$\sigma = \frac{\dot{\delta}}{\omega} \tag{2.3.35}$$

Dividing both sides of eq. (2.3.31) by ω (ω = constant) yields

$$\frac{\ddot{\delta}}{\omega} = \frac{\pi f}{\omega H}(P_m - P_e) \tag{2.3.36}$$

Since

$$\omega = 2\pi f \tag{2.3.37}$$

substituting (2.3.35) into (2.3.36) yields

$$\frac{d}{dt}(\sigma) = \frac{P_m - P_e}{2H} \tag{2.3.38}$$

From eq. (2.3.38),

$$\int_{\sigma(n)}^{\sigma(n+1)} d\sigma = \frac{1}{2H}\int_{t}^{t+\Delta t}(P_m - P_e)dt \tag{2.3.39}$$

For the period of time of interest in transient stability analyses, the mechanical load on the motors can be assumed constant. Furthermore, if the electrical torque-producing power in the motor is clamped constant

throughout the iteration, that is,

$$P_e(t) = P_e(n) \text{ for } n\Delta t \leq t \leq (n+1)\Delta t \tag{2.3.40}$$

then the solution to equation (2.3.39) becomes

$$\sigma(n+1) = \sigma(n) + \frac{\Delta t}{2H}(P_m - P_e(n)) \tag{2.3.41}$$

Equations (2.3.29) and (2.3.41), then, describe the mathematical model used in this study to represent an arbitrary induction motor. The slip equation is solved first, and with this value of slip, a new value of the transient emf E' is computed. One set of these equations must be solved at every load bus serving induction machines. The subscript indicating the machine number will now be replaced so the final model for the ith machine becomes

$$\sigma_i(n+1) = \sigma_i(n) + \frac{\Delta t}{2H_i}(P_{mi} - P_{ei}(n)) \tag{2.3.42}$$

$$\begin{bmatrix} a'_i(n+1) \\ b'_i(n+1) \end{bmatrix} = \hat{\Phi}_{\sim i}(n) \begin{bmatrix} a'_i(n) \\ b'_i(n) \end{bmatrix} + \hat{\theta}_{\sim i}(n) \begin{bmatrix} \hat{a}_i(n) \\ \hat{b}_i(n) \end{bmatrix} \tag{2.3.43}$$

2.4 Generator Models

The synchronous generator is usually the most carefully studied single piece of equipment that makes up a typical power system. Many mathematical models exist for representing the behavior of this machine. Since the time constants of the governor, exciter and other devices are long compared to the duration of the transient stability period, neglecting saliency effect the generators in these studies can be represented by an emf in series with an impedance (Fig. 2.4.1), where:

$\bar{V}_i$ = voltage of the ith bus,

$\bar{E}_i$ = emf of the ith generator,

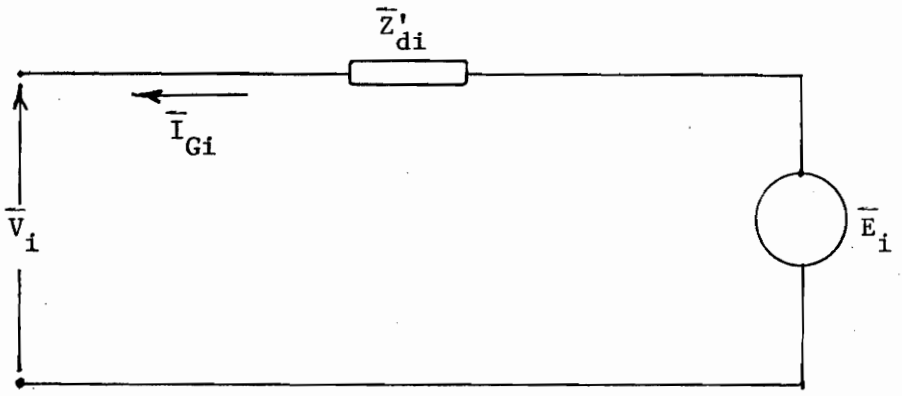

Fig. 2.4.1 Equivalent Circuit of Synchronous Machine Under Transient Conditions

$\bar{Z}'_{di}$ = transient impedance of the ith generator,

$\bar{S}_{Gi}$ = complex power generated by the ith generator.

It is assumed that the generator numbering coincides with the bus numbering. Unlike the induction machine, where the emf was described by a complex-coefficient linear differential equation, the emf of the ith synchronous generator is given, at any time, by:

$$\bar{E}_i = \bar{V}_i + \bar{Z}'_{di}\left(\frac{\bar{S}_{Gi}}{\bar{V}_i}\right)^* \qquad (2.4.1)$$

The rotating masses, however, are modeled exactly as they were in the induction machine. For the ith generator, then, the motion of the rotor can be represented mathematically as:

$$\ddot{\delta}_i = \frac{-D_i \pi f}{H_i}\dot{\delta}_i + \frac{\pi f}{H_i}P_{ai} \qquad (2.4.2)$$

where, as before,

δ_i = the electrical angle between the rotor of the ith generator and a synchronously rotating reference,

D_i = damping coefficient of the ith generator,

H_i = inertia constant of the ith generator,

f = nominal frequency,

$\pi \cong 3.14159$

and the accelerating power at bus i (P_{ai}) is defined as:

$$P_{ai} = P_{Ti} - P_{Ei}$$

where

P_{Ti} = turbine power at the ith generator

$= P^{\circ}_{Ei}$

P_{Ei} = electrical power generated at the ith generator.

The turbine power is analogous to the mechanical load power on the induction motor. Like the mechanical load, the turbine power is assumed constant throughout the transient stability period. The electrical power is given, at each point in time, by

$$P_{Ei} = \mathrm{Re}\left[\frac{1}{(Z'_{di})^*}(|E_i|^2 - \bar{E}_i \bar{V}_i^*)\right] \tag{2.4.3}$$

The swing equation (2.2.3) can be expressed as two coupled first-order equations, that is,

$$\frac{d}{dt}\delta_i = \dot{\delta}_i \tag{2.4.4}$$

$$\frac{d}{dt}\dot{\delta}_i = \frac{-D_i \pi f}{H_i}\dot{\delta}_i + \frac{\pi f}{H_i}P_{ai} \tag{2.4.5}$$

In matrix form, these become

$$\frac{d}{dt}\begin{bmatrix}\delta_i \\ \dot{\delta}_i\end{bmatrix} = \begin{bmatrix}0 & 1 \\ 0 & \frac{-D_i \pi f}{H_i}\end{bmatrix}\begin{bmatrix}\delta_i \\ \dot{\delta}_i\end{bmatrix} + \begin{bmatrix}0 \\ \frac{\pi f}{H_i}\end{bmatrix} \tag{2.4.6}$$

Assuming the accelerating power is clamped during the iteration time step Δt, eq. (2.4.6) represents a linear system of equations in the standard form

$$\dot{\underline{x}} = \underline{A}\underline{x} + \underline{B}\underline{u} \tag{2.4.7}$$

where

$$\underline{x} = \begin{bmatrix}\delta_i \\ \dot{\delta}_i\end{bmatrix} \tag{2.4.8}$$

$$\underset{\sim}{A} = \begin{bmatrix} 0 & 1 \\ 0 & \dfrac{-D_i \pi f}{H_i} \end{bmatrix} \tag{2.4.9}$$

$$\underset{\sim}{B} = \begin{bmatrix} 0 \\ \dfrac{\pi f}{H_i} \end{bmatrix} \tag{2.4.10}$$

Again, many ways exist for solving this system. Like the solution to the induction motor emf, Laplace transforms were used and the expression for the state of the ith induction machine at the (n+1)th iteration is given by:

$$\begin{bmatrix} \delta_i(n+1) \\ \dot{\delta}_i(n+1) \end{bmatrix} = \underset{\sim}{\Phi}_i \begin{bmatrix} \delta_i(n) \\ \dot{\delta}_i(n) \end{bmatrix} + \underset{\sim}{\Theta}_i P_{ai}(n) \tag{2.4.11}$$

For damped generators,

$$\underset{\sim}{\Phi}_i = \begin{bmatrix} 1 & \dfrac{1}{\lambda_i}(e^{\lambda_i \Delta t} - 1) \\ 0 & e^{\lambda_i \Delta t} \end{bmatrix} \tag{2.4.12}$$

and

$$\underset{\sim}{\Theta}_i = \frac{1}{D_i} \begin{bmatrix} \dfrac{1}{\lambda_i}(1 - e^{\lambda_i \Delta t}) + \Delta t \\ (1 - e^{\lambda_i \Delta t}) \end{bmatrix} \tag{2.4.13}$$

where

$$\lambda_i = \frac{-D_i \pi f}{H_i} \tag{2.4.14}$$

For undamped generators, the state transition matrix phi is given by

$$\underset{\sim}{\Phi}_i = \begin{bmatrix} 1 & \Delta t \\ 0 & 1 \end{bmatrix} \tag{2.4.15}$$

and the theta matrix becomes

$$\underset{\sim}{\Theta}_i = \begin{bmatrix} \frac{\omega}{H_i}(\Delta t)^2 \\ \frac{\omega}{2H_i}(\Delta t) \end{bmatrix} \tag{2.4.16}$$

Unlike the induction machines, the $\underset{\sim}{\Phi}$ and $\underset{\sim}{\Theta}$ matrices for the synchronous machines are a function only of the time increment Δt. These matrices, therefore, need only be evaluated once at the beginning of the run.

2.5 Solution Method

In this section, the models discussed will be integrated into a routine to analyze the transient stability of electric power systems. Figure (2.5.1) shows an abridged flowchart detailing the solution method used. Steps such as reading in data, initializing variables, printing error messages, and others not pertinent to the discussion have been omitted. Each step of the flowchart is detailed below:

1. Determine the least-squares coefficients for any load modeled as a polynomial; that is, determine $(a_o)_j$, $(a_1)_j$, ..., $(a_4)_j$ and $(b_o)_j$, $(b_1)_j$, ..., $(b_4)_j$, $\quad j = 1, \ldots, m$
   where m = number of loads represented by curves.
2. Perform a loadflow to determine the state of the system before the fault occurred. Polar form Newton-Raphson loadflow was used in this study.

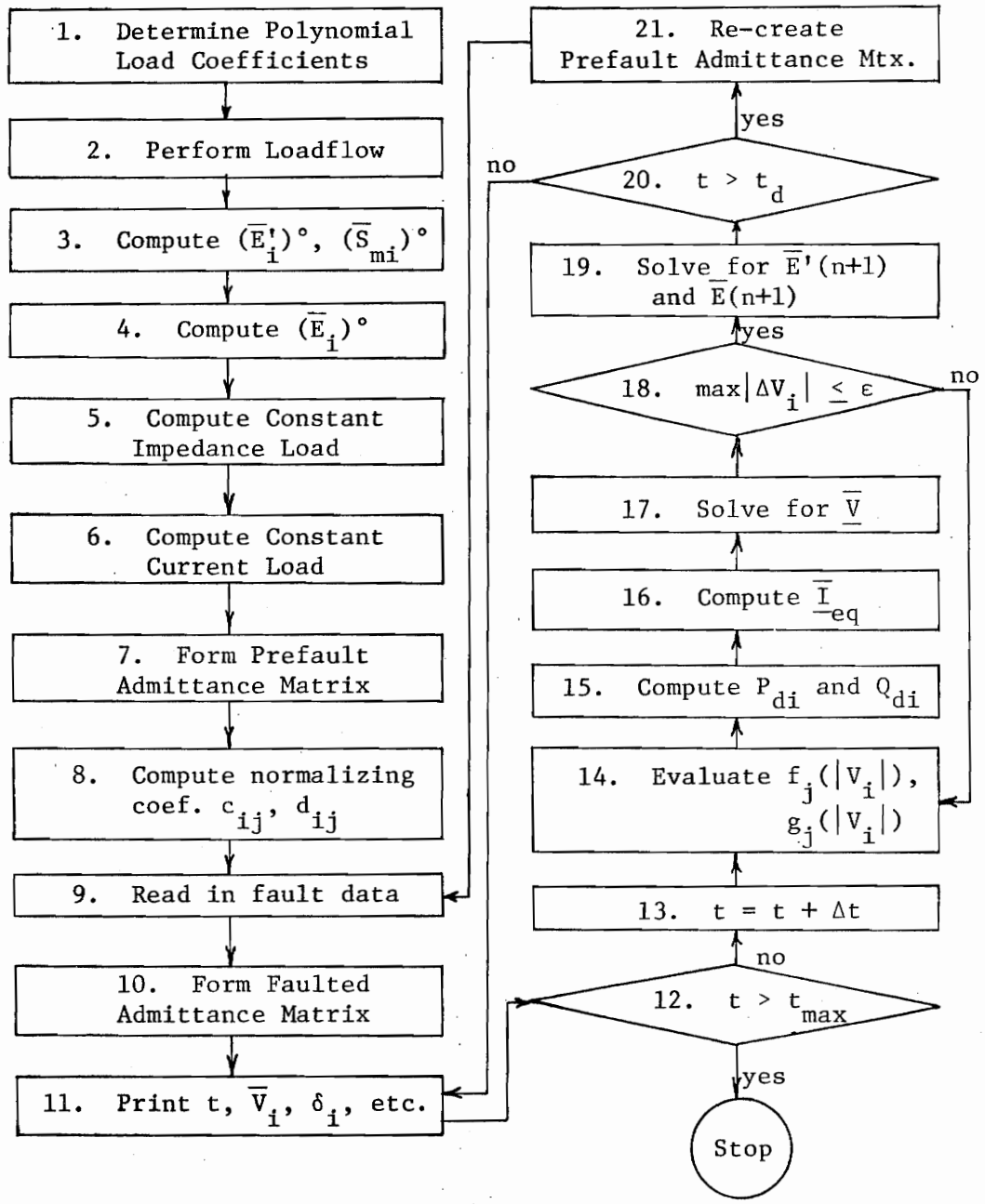

Fig. 2.5.1 Flowchart of Solution Algorithm

3. In the input data, the complex power drawn by induction machines is lumped with the power drawn by constant impedance loads. More on this in Step 5. Given the machine particulars and initial slip, the prefault current and power drawn by the induction machine at bus i is given by

$$\bar{I}_{mi} = \bar{V}_i/(\bar{Z}_{ind})_i \text{ and} \qquad (2.5.1)$$

$$\bar{S}_{mi} = \bar{V}_i\bar{I}^*_{mi} \qquad (2.5.2)$$

where $(\bar{Z}_{ind})_i$ = input impedance of the steady-state model (Fig. 2.3.1),

$\bar{I}_{mi}$ = current drawn by the ith motor, and

$\bar{S}_{mi}$ = complex power drawn by the ith motor.

Once the power drawn by the machine has been determined, the initial equivalent transient emf $\bar{E}'$ is computed as follows (Fig. 2.3.2):

$$(\bar{E}'_i)^\circ = \bar{V}_i - \bar{I}_{mi}(r_{si} + jX'_i) \qquad (2.5.3)$$

4. The initial emf $\bar{E}$ of the synchronous machine at bus i is calculated in a method analogous to the method above; that is,

$$(\bar{E}_i)^\circ = \bar{V}_i + \left(\frac{\bar{S}_{Gi}}{\bar{V}_i}\right)^*\bar{Z}'_{di} \qquad (2.5.4)$$

5. The assumed induction motor load was lumped with the constant impedance load so that the loadflow could be performed. Once the bus voltage is determined and the induction motor power is solved for, this power must be subtracted from the constant impedance load power in order to maintain a power balance. The operation indicated in the flowchart is

$$\bar{S}_{Zi} = \bar{S}_{Zi}(\text{l.f.}) - \bar{S}_{mi} \qquad (2.5.5)$$

where $\bar{S}_{Zi}$ = power drawn by constant impedance load at bus i, and

$\bar{S}_{Zi}$(1.f.) = quantity used in performing prefault loadflow.

6. The constant current portion of the load is simply given by

$$\bar{I}_{cc,i} = \left(\frac{\bar{S}^{\circ}_{cc,i}}{\bar{V}^{\circ}_{i}}\right)^{*} \tag{2.5.6}$$

where the subscript "cc,i" indicates the constant current portion of the quantity at bus i.

7. The bus admittance matrix must now be modified to account for the constant impedance loads, the induction motors, and the synchronous generators. Constant impedance loads are represented by an equivalent shunt admittance added to the diagonal element of $\bar{Y}_{bus}$. As seen in section 2.2, the value of this equivalent admittance for the constant impedance load at bus i ($\bar{Y}_{Zi}$) is given by

$$\bar{Y}_{Zi} = (\bar{S}_{Zi})^{*}/|V^{\circ}_{i}|^{2} \tag{2.5.7}$$

The induction motors and synchronous generators are represented by their respective Norton equivalents (Figs. 2.5.2, 2.5.3) where

$$\bar{Y}_{Mi} = \frac{1}{r_s + jX'} \tag{2.5.8}$$

$$\bar{I}_{Mi} = \bar{E}'_i \bar{Y}_{Mi} \tag{2.5.9}$$

$$\bar{Y}_{Gi} = \frac{1}{\bar{Z}'_{di}} \tag{2.5.10}$$

$$\bar{I}_{Gi} = \bar{E}_i \bar{Y}_{Gi} \tag{2.5.11}$$

The generator and motor shunt admittances at the ith bus are also added to the ith diagonal element at $\bar{Y}_{bus}$; that is,

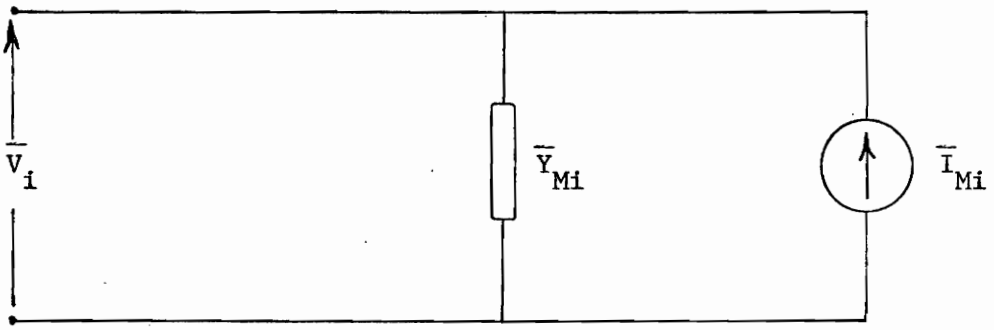

Fig. 2.5.2 Norton Equivalent of Induction Machine at Bus i Under Transient Conditions

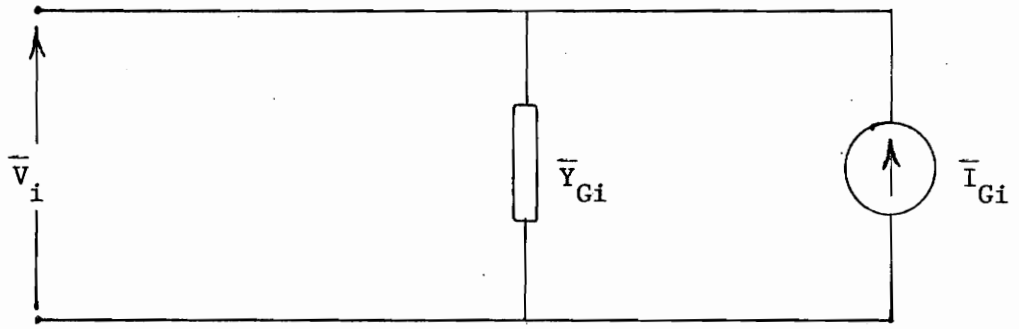

Fig. 2.5.3 Norton Equivalent of Synchronous Generator at Bus i Under Transient Conditions

$$\bar{Y}^{o}_{i,i} = \bar{Y}_{i,i}(1.f.) + \bar{Y}_{Zi} + \bar{Y}_{Mi} + \bar{Y}_{Gi} \qquad (2.5.12)$$

where the argument (1.f.) indicates the quantity used in performing the loadflow and the superscript "o" indicates a prefault quantity.

8. At this point, the only thing needed before proceeding with the fault analysis is the evaluation of the normalizing coefficients for the loads modeled as polynomials in V. These are given by

$$c_{ij} = \frac{P^{o}_{ij}}{f_j(|V_i|)} \qquad \begin{matrix} i = 1, \ldots, n \\ j = 1, \ldots, m \end{matrix}$$

$$d_{ij} = \frac{Q^{o}_{ij}}{g_j(|V_i|)} \qquad \begin{matrix} i = 1, \ldots, n \\ j = 1, \ldots, m \end{matrix}$$

where n = number of buses in the system, and

m = number of loads represented as polynomials.

9. Fault data is now read in:

   a. Type 1 - three-phase admittance to ground at a bus

      Type 2 - generator tripped

      Type 3 - line opened at both ends.

   b. Location - location of the fault

   c. Duration - time at which fault is removed as measured from t=0 (t_d)

10. The bus admittance matrix is once again modified to model the effect of the fault. For a three-phase admittance to ground at bus i, the value of the fault admittance is added to the ith diagonal element of $\bar{Y}_{bus}$; that is,

$$\bar{Y}^{f}_{i,i} = \bar{Y}^{o}_{i,i} + \bar{Y}_{f} \qquad (2.5.13)$$

where $\bar{Y}_f$ is defined to be the fault admittance and the superscript "f" indicates a faulted quantity. For a generator trip at the ith bus, the Norton generator admittance is subtracted from the ith diagonal element of $\bar{\bar{Y}}_{bus}$, that is,

$$\bar{\bar{Y}}^f_{i,i} = \bar{\bar{Y}}^\circ_{i,i} - \bar{Y}_{Gi} \qquad (2.5.14)$$

For a tripped line, the series admittance of the line is subtracted from the transfer terms of $\bar{\bar{Y}}_{bus}$ and the shunt admittance of the line is subtracted from the diagonal terms corresponding to the end points of the lines; that is, if line k connects buses i and j,

$$\bar{\bar{Y}}^f_{i,j} = \bar{\bar{Y}}^\circ_{i,j} - \frac{1}{\bar{Z}_{ser,k}} \qquad (2.5.15)$$

$$\bar{\bar{Y}}^f_{j,i} = \bar{\bar{Y}}^\circ_{j,i} - \frac{1}{\bar{Z}_{ser,k}} \qquad (2.5.16)$$

$$\bar{\bar{Y}}^f_{i,i} = \bar{\bar{Y}}^\circ_{i,i} - \bar{Y}_{sh,k} \qquad (2.5.17)$$

$$\bar{\bar{Y}}^f_{j,j} = \bar{\bar{Y}}^\circ_{j,j} - \bar{Y}_{sh,k} \qquad (2.5.18)$$

where transmission lines are assumed to be modeled by pi equivalent circuits and

$\bar{Z}_{ser,k}$ = series impedance of line k,

$\bar{Y}_{sh,k}$ = half the total shunt admittance of line k.

11. At this point, all quantities of interest, such as bus voltages and generator angles, are printed out.

12. Has the maximum solution time elapsed?

    a. Yes - stop.

    b. No - continue.

13. Increment time by the timestep.

14. Evaluate polynomial loads; that is, compute

$$f_j(|V_i|) = (a_o)_j + (a_1)_j|V_i| + \ldots + (a_4)_j|V_i|^4$$

$$g_j(|V_i|) = (b_o)_j + (b_1)_j|V_i| + \ldots + (b_4)_j|V_i|^4$$

for $j = 1, \ldots, m$ and

i = load buses.

15. Compute real and reactive power drawn at each load bus by polynomial loads as follows:

$$P_{di} = \sum_{j=1}^{m} c_{ij} f_j(|V_i|)$$

$$Q_{di} = \sum_{j=1}^{m} d_{ij} g_i(|V_i|)$$

for all load buses.

16. Calculate an equivalent injected current source $\bar{I}_{eq}$ where

$$(\bar{I}_{eq})_i = \bar{I}_{Gi} + \bar{I}_{Mi} - \frac{P_{di} + jQ_{di}}{\bar{V}_i} - \bar{I}_{cc,i}, \quad i=1, \ldots, n \qquad (2.5.19)$$

Note 1: $\bar{I}_{Mi} = 0$ if there is no motor at bus i.

$P_{di} = Q_{di} = 0$ if there are no polynomial loads at bus i.

$\bar{I}_{cc,i} = 0$ if there is no constant current load at bus i.

Note 2: $\bar{I}_{Gi}$ is set to zero if the ith generator is tripped.

17. Solve the following algebraic system for a new voltage profile:

$$\underset{\sim}{\bar{Y}}^{f}_{bus}\, \bar{V} = \bar{I}_{eq} \qquad (2.5.20)$$

18. Since the polynomial portion of $\bar{I}_{eq}$ represents a voltage-controlled current source, the new voltage profile must be arrived at by

iteration. This step, then checks for convergence:

$$\max_{1 \leq i \leq n} \left|\Delta V_i\right| \leq \varepsilon \tag{2.5.21}$$

where $\Delta\bar{V}_i$ is defined as the change in the voltage at bus i induced by eq. (2.5.20). If the inequality holds, continue. If the inequality does not hold, go to step 14.

19. With the new voltage profile, solve for new values of $\bar{E}_i$ and $\bar{E}'_i$. Solving for the slip first:

$$\sigma_i(n+1) = \sigma_i(n) + \frac{\Delta t}{2H_i}(P_{mi} - P_{ei}(n)) \tag{2.3.42}$$

where
$$P_{ei} = \mathrm{Re}\{\bar{E}'_i \bar{I}_{mi}\} \tag{2.5.22}$$

and
$$P_{mi} = \text{prefault mechanical load}$$
$$= \mathrm{Re}\{(\bar{E}'_i)^{\circ}\bar{I}^{\circ}_{mi}\} \tag{2.5.23}$$

Now that the slip has been determined, the $\hat{\Phi}_i$ and $\hat{\Theta}_i$ matrices can be evaluated and the real and imaginary parts of the emf E' at the (n+1)th iteration are given by

$$\begin{bmatrix} a'_i(n+1) \\ b'_i(n+1) \end{bmatrix} = \hat{\Phi}_i(n) \begin{bmatrix} a'_i(n) \\ b'_i(n) \end{bmatrix} + \hat{\Theta}_i(n) \begin{bmatrix} \hat{a}_i(n) \\ \hat{b}_i(n) \end{bmatrix} \tag{2.3.43}$$

where the quantities $\hat{a}_i$ and $\hat{b}_i$ are defined in Section 2.3 (eqs. 2.3.18) and

$$\bar{E}'_i(n+1) = a'_i(n+1) + jb'_i(n+1) \tag{2.5.24}$$

Now the new generator emf's $\bar{E}_i$ are solved for. Since the magnitude is assumed constant during the transient stability period, only the new angles δ_i and angular velocities $\dot{\delta}_i$ need be solved for:

$$\begin{bmatrix} \delta_i(n+1) \\ \dot{\delta}_i(n+1) \end{bmatrix} = \underset{\sim}{\Phi}_i \begin{bmatrix} \delta_i(n) \\ \dot{\delta}_i(n) \end{bmatrix} + \underset{\sim}{\Theta}_i P_{ai}(n) \qquad (2.4.11)$$

where $\underset{\sim}{\Phi}_i$ and $\underset{\sim}{\Theta}_i$ are defined in section 2.4 and need only be evaluated once since they are a function only of the time step Δt. The accelerating power is given by

$$P_{ai}(n) = P_{Ti} - P_{Ei}(n) \qquad (2.5.25)$$

The electrical power, since it is a function of bus voltage (eq. 2.4.5), must be evaluated at each iteration. The turbine power is assumed constant throughout the transient stability period and is given by

$$P_{Ti} = P^{\circ}_{Ei} \qquad (2.5.26)$$

Note: If the fault is a generator trip,

$$P_{ai}(n) = P_{Ti} \qquad (2.5.27)$$

since no electrical power is delivered by the generator.

20. Has the fault time elapsed? $(t > t_d)$

    a. No - go to step 11.

    b. Yes - continue.

21. Reconstruct the prefault admittance matrix by reversing operations performed in step 10. After the prefault admittance matrix is obtained, go to step 9.

These steps outline the procedure used in solving for the generator swing curves.

3.0 RESULTS

3.1 Introduction

In this chapter, a specific fault was analyzed under six different loading conditions:

1. loads modeled as constant-impedance loads,
2. loads modeled as constant-current loads,
3. loads modeled as a combination of constant impedance and induction motors with the induction motor inertia constant H = 0.03,
4. Same as 3 above but H = 3.0,
5. Same as 3 above but H = 300,
6. loads modeled as a combination of constant impedance, induction motor, air conditioning, and fluorescent lighting with induction motor inertia constant H = 3.0.

Swing curves and load bus voltage curves obtained from analyzing the six cases outlined above are included and discussed in section 3.3 and section 3.4, respectively. The next section describes the system under study.

3.2 Test Data

The nine-bus system used in this study (Fig. 3.2.1) is from Anderson and Fouad's book Power System Control and Stability [4]. Pertinent generator data is tabulated in Table (3.2.1) and induction motor data is in Table (3.2.2).

When the effect of induction machines is studied, all three load buses are assumed to serve this type of device. Table (3.2.3) shows

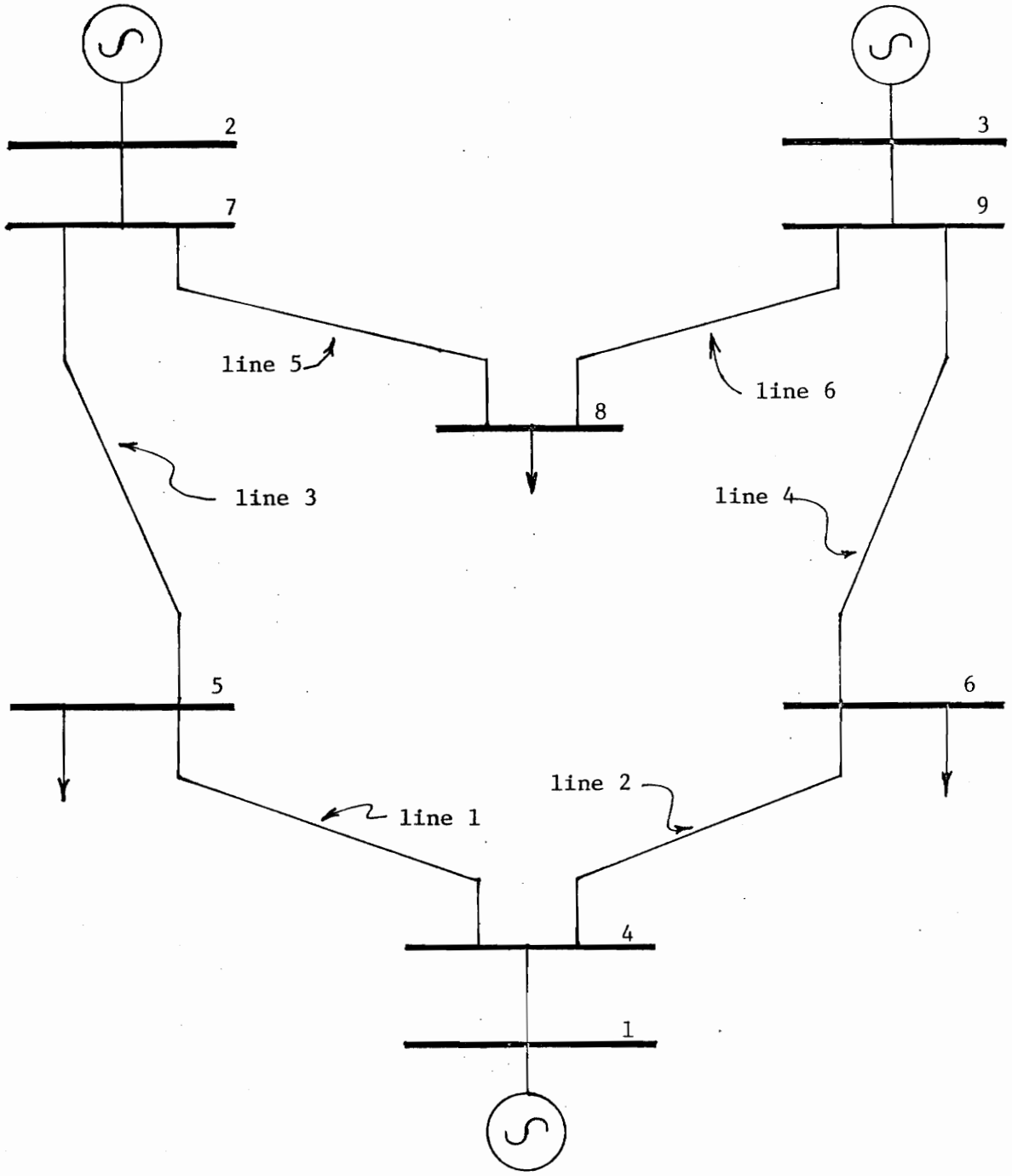

Fig. 3.2.1 Test System

Table 3.2.1 - Generator Data

GENERATOR NUMBER	TRANSIENT ADMITTANCE	INERTIA CONSTANT	DAMPING COEFFICIENT
1	0.0000 - j16.4474	23.64	0.00
2	0.0000 - j 8.3472	6.40	0.00
3	0.0000 - j 5.5157	3.01	0.00

Table 3.2.2 - Induction Motor Data [3]

Stator resistance	$r_s = 0.0450$
Stator reactance	$x_s = 0.0750$
Rotor resistance	$r_r = 0.0450$
Rotor reactance	$x_r = 0.0750$
Magnetizing reactance	$x_m = 3.0000$
Initial slip	$\sigma^\circ = 0.0210$

the amount of active and reactive power drawn at load buses serving constant impedance and induction motor loads. Table (3.2.4) shows the mixture of active and reactive power drawn from buses serving constant impedance, induction motor and polynomial curve-fit loads. Air conditioners were assumed to be quasi-static devices. This allowed representation of their characteristics as a polynomial in $|V|$.

The data used to simulate load behavior with a polynomial is similar to that obtained by Adler and Mosher [1]. The devices which were modeled in this fashion were fluorescent lights and air conditioners, the characteristics of which are depicted in Fig. (3.2.2) and Fig. (3.2.3), respectively. The curves indicate the polynomial approximation and the asterisks indicate experimental data points.

The fault under study is a three-phase admittance of j1000 per units between bus 7 and ground which is cleared in $0.8\overline{3}$ seconds by opening line 3 at both ends.

3.3 Swing Curves

The plots of the electrical angles of synchronous generator rotors as measured from a synchronously rotating frame of reference versus time will be referred to as swing curves. These swing curves give the system designer an idea of the effects of a disturbance on the particular system in question.

In order to obtain the swing curves, certain information about the customers served by the utility must be obtained in order to model the load accurately. If this information is unavailable, the loads are generally modeled as constant impedance loads or a combination of constant impedance and constant current.

Table 3.2.3 - Load Power Distribution at
Buses Serving Induction Motors and Constant Impedance Loads

BUS NUMBER	5	6	8
CONST. Z POWER	0.8148 + j0.1609	0.4498 - j0.0508	0.5468 - j0.0031
IND. MOTOR POWER	0.4352 + j0.3391	0.4502 + j0.3508	0.4532 + j0.3531
TOTAL LOAD POWER	1.2500 + j0.5000	0.9000 + j0.3000	1.0000 + j0.3500

Table 3.2.4 - Load Power Distribution at Buses Serving Mixed Loads

BUS NUMBER	5	6	8
CONST. Z POWER	0.1148 - j0.1191	0.2499 - j0.0008	0.3468 - j0.0469
IND. MOTOR POWER	0.4352 + j0.3391	0.4501 + j0.3508	0.4532 + j0.3531
AIR CONDITIONING	0.5000 + j0.3300	0 + j0	0 + j0
FL. LIGHTING	0.2000 - j0.0500	0.2000 - j0.0500	0.2000 - j0.0500
TOTAL LOAD POWER	1.2500 + j0.5000	0.9000 + j0.3000	1.0000 + j0.3500

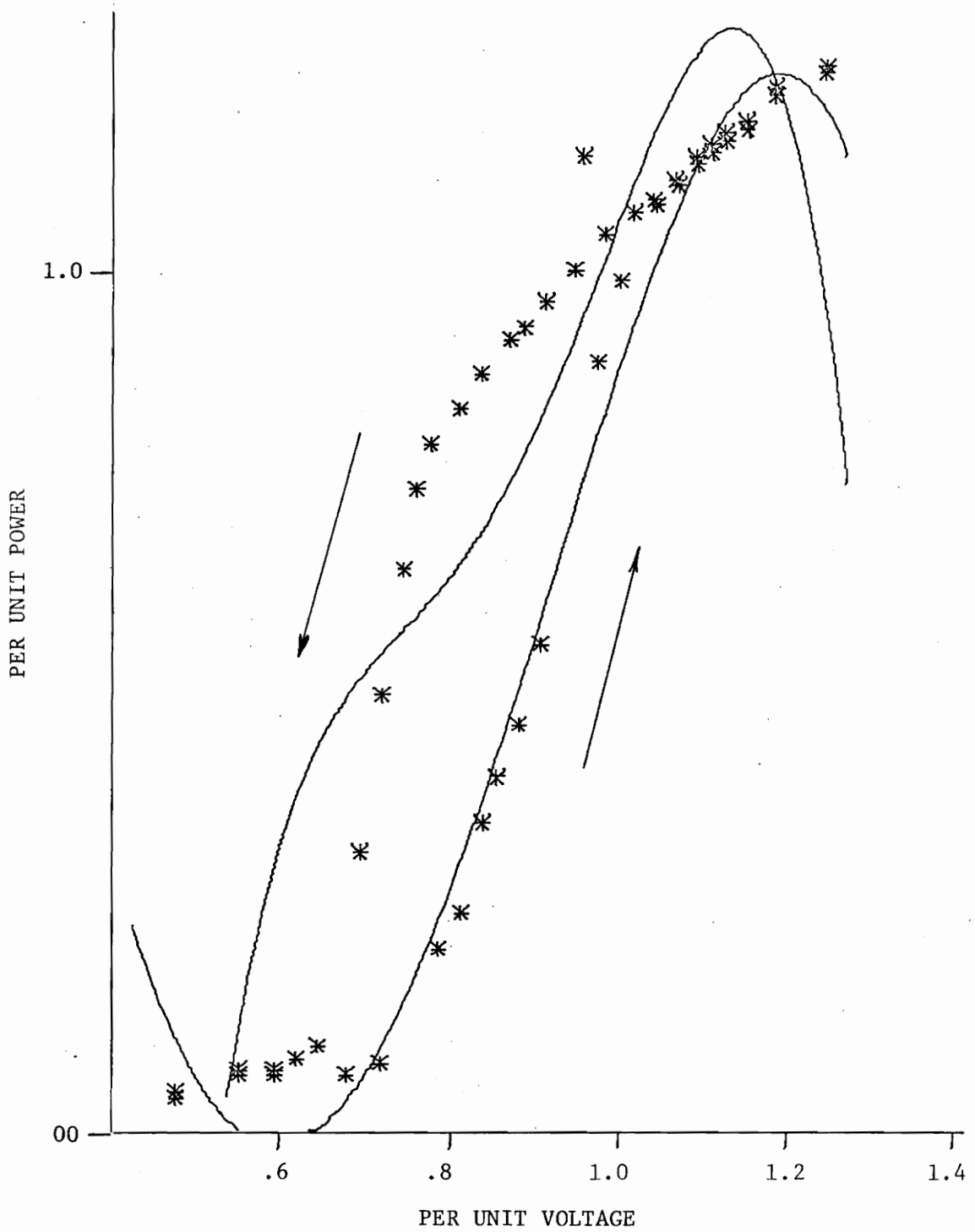

Fig. 3.2.2 - Fluorescent Light Characteristics
a-Active Power

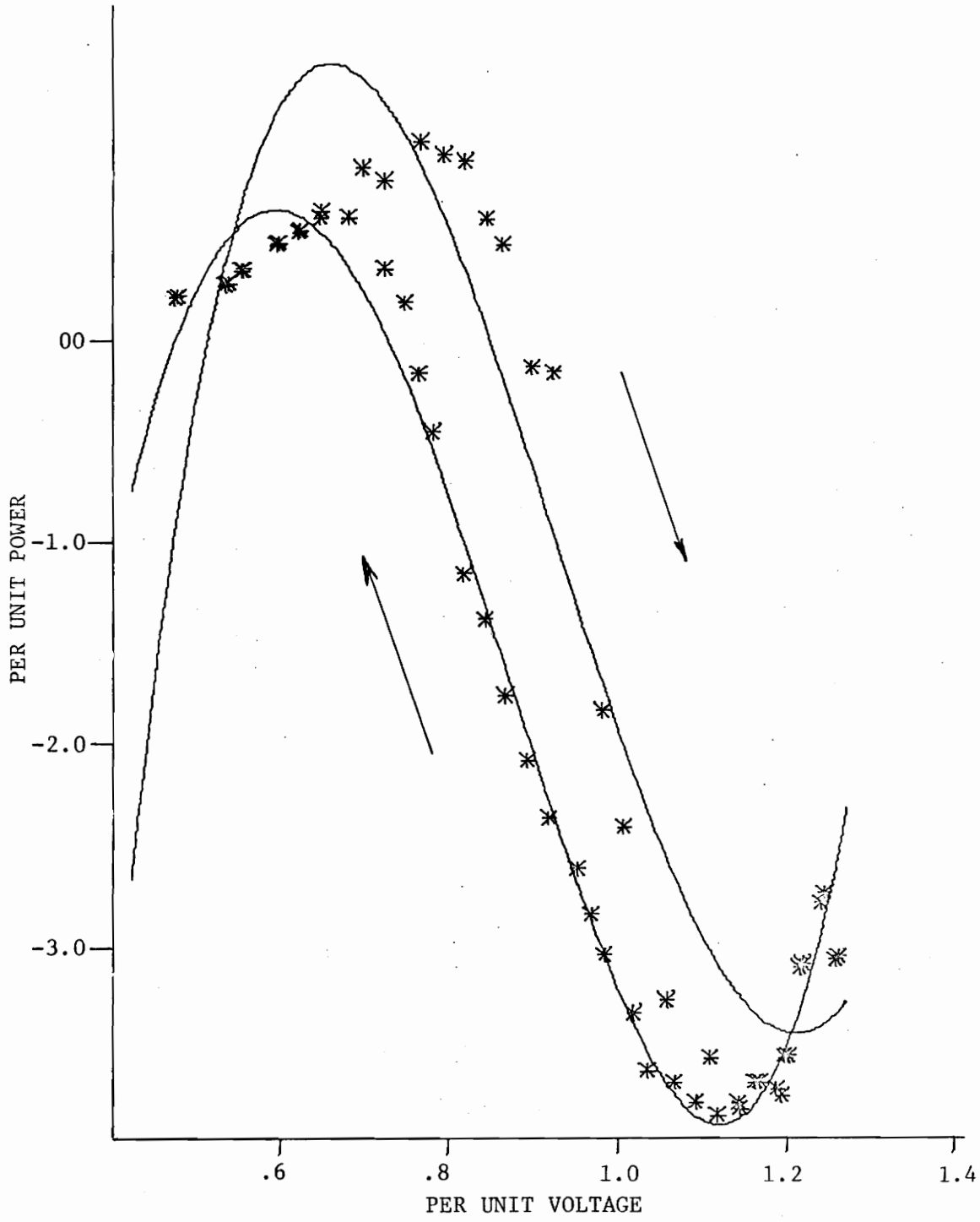

Fig. 3.2.2 - Fluorescent Light Characteristics
b-Reactive Power

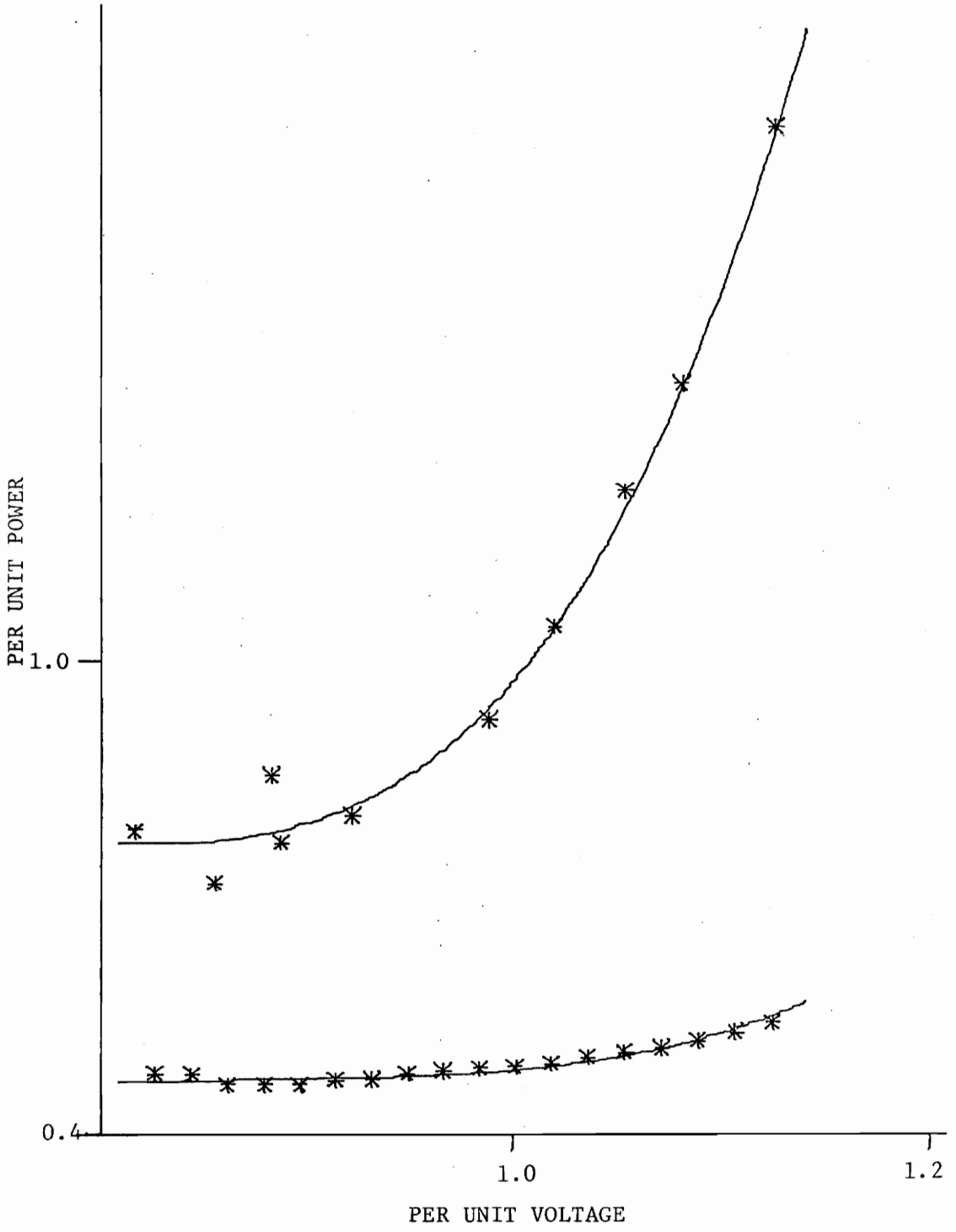

Fig. 3.2.3 - Air Conditioning Characteristics

In this section several swing curves (Fig. 3.3.1 to Fig. 3.3.6) will be compared. The only difference between them is the method of load modeling.

The most common type of load model in use today is the constant impedance model. Because of this, the results obtained by modeling loads in this way will be referred to as the "base case". Fig. (3.3.1) depicts the "base case" swing curves, that is, the curves describing the relative position of the generator rotors when the loads are all modeled as constant impedances.

Another method of modeling loads is to assume that they draw prefault current throughout the solution time. Fig. (3.3.2) depicts the swing curves of the generators when loads are modeled in this manner. This method of load modeling causes the generators to swing much faster than the constant impedance case in order to satisfy the algebraic constraints on the system. This situation clearly represents a more unstable case than the one previously mentioned.

Fig. (3.3.3) through Fig. (3.3.5) represent a combination of induction motor and constant impedance loads. The quantities of each type of load are listed in the previous section (Table 3.2.3). Since the induction motors are modeled dynamically, an inertia constant associated with these loads must be arrived at. This model, however, is for a conglomerate of induction machines. This makes obtaining a single value for the inertia constant an impossibility. The figures mentioned above, then, all depict the same fractional loading but have different induction motor inertia constants.

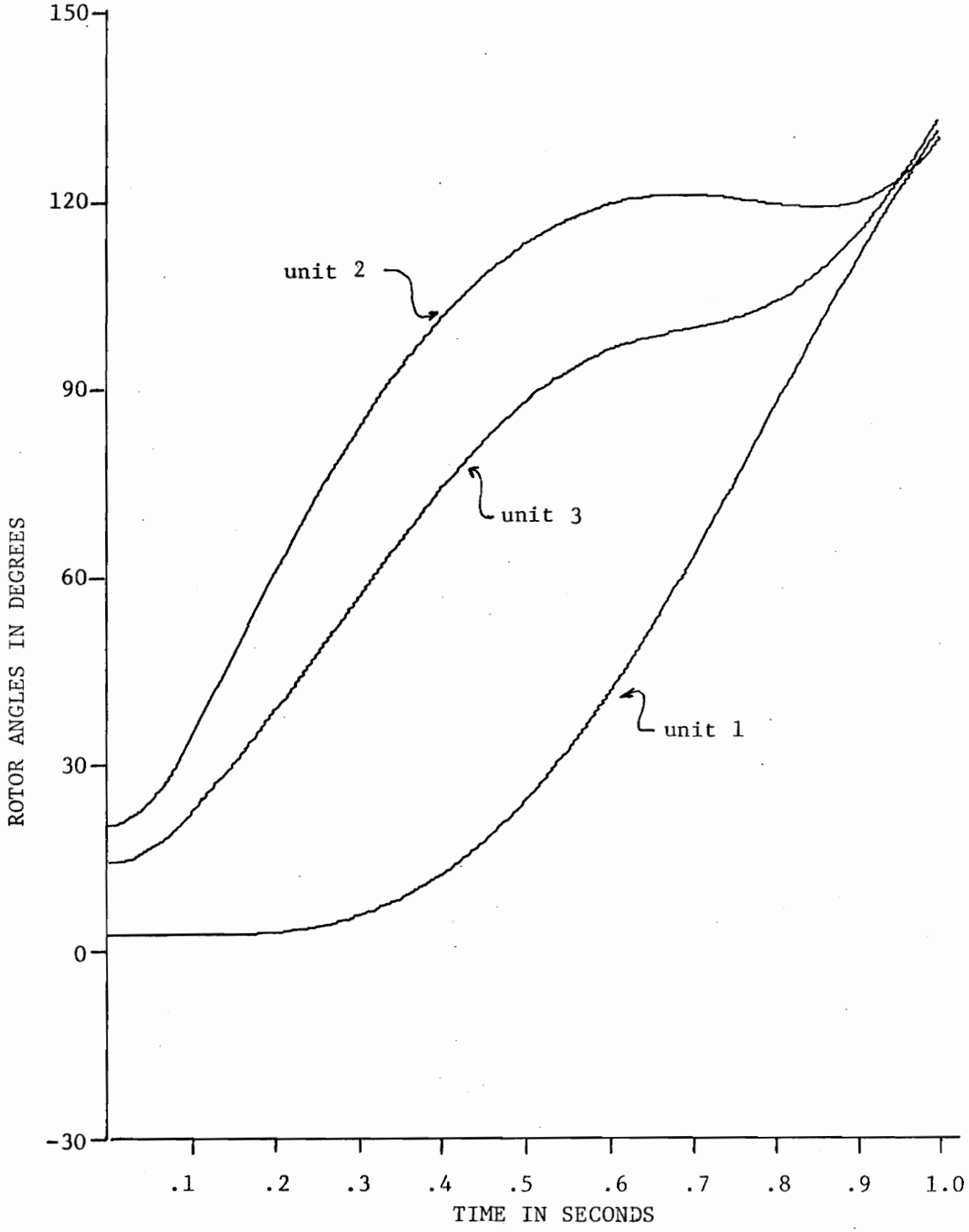

Fig. 3.3.1 Swing Curves
Constant Impedance Loads

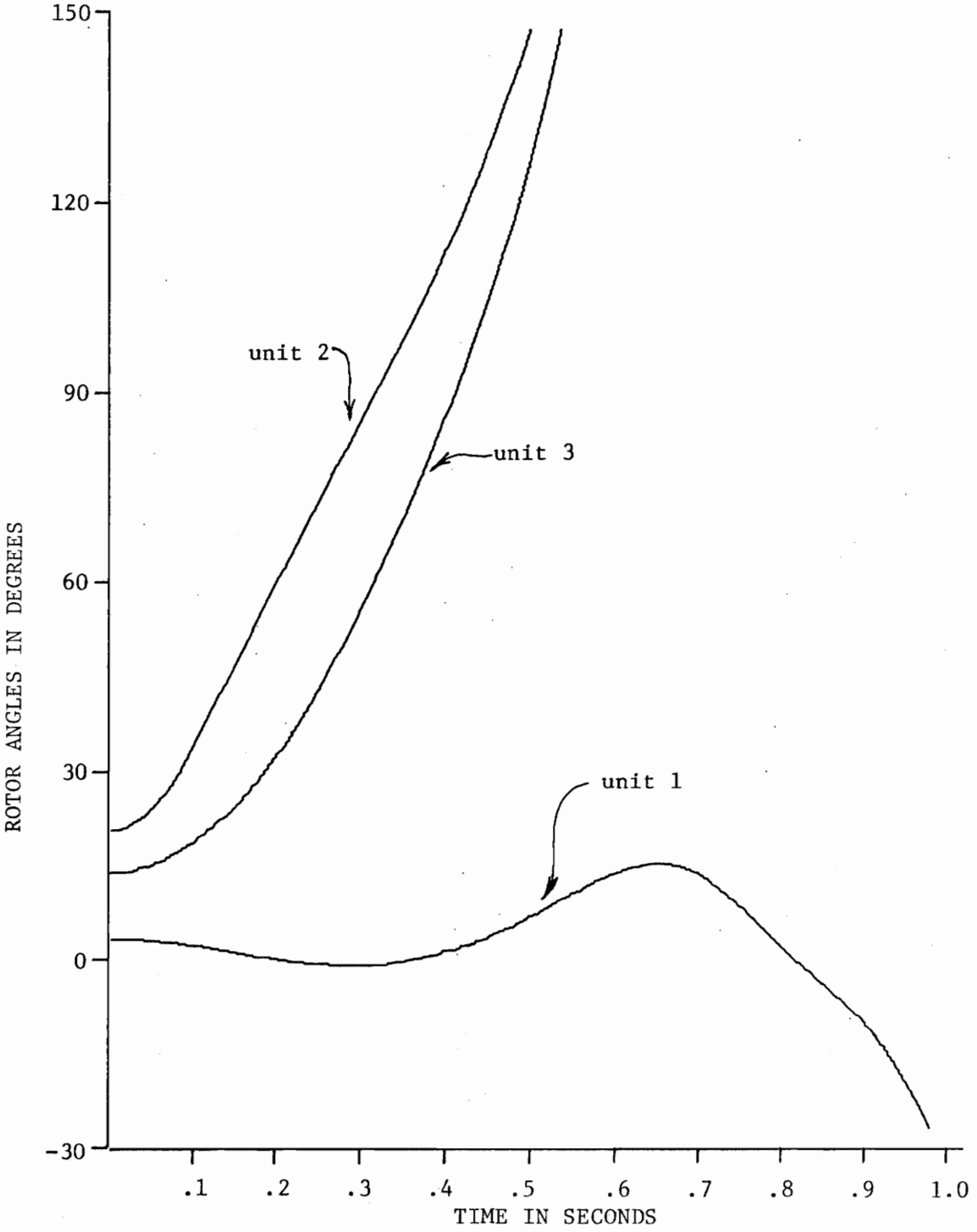

Fig. 3.3.2 Swing Curves
Constant Current Loads

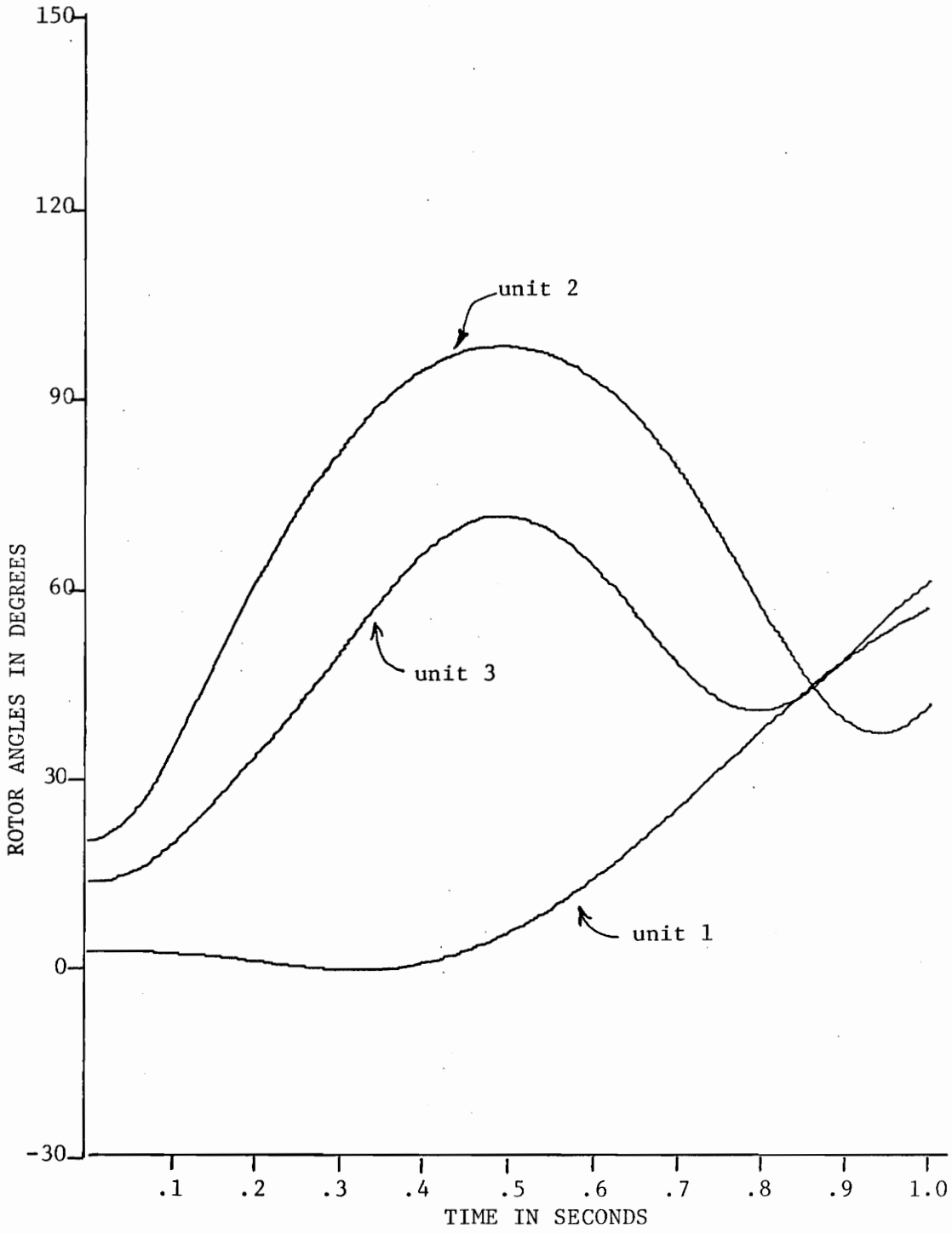

Fig. 3.3.3 Swing Curves
Induction Motors and Constant Impedance Loads (H = 0.03)

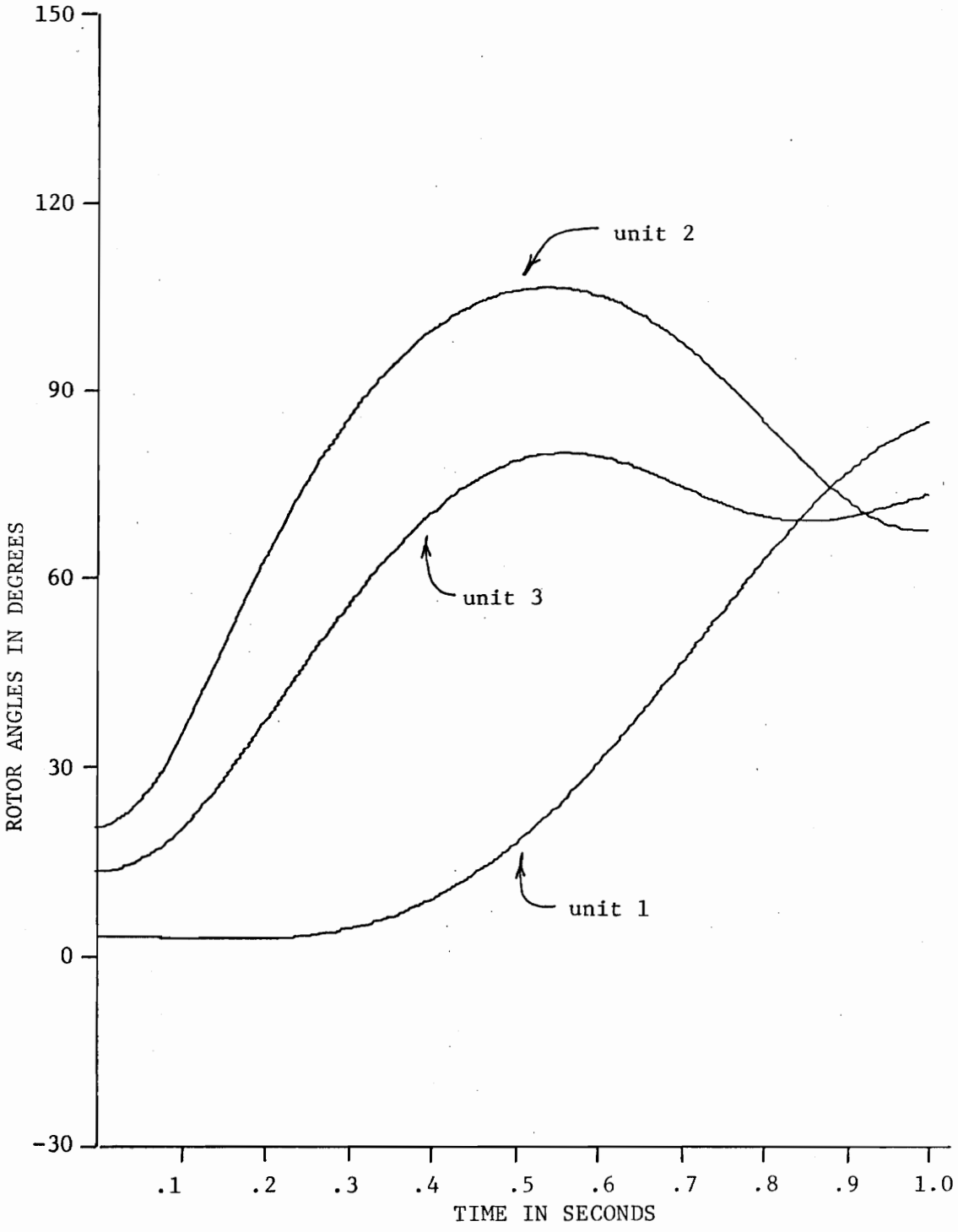

Fig. 3.3.4 Swing Curves
Induction Motors and Constant Impedance Loads (H = 3.0)

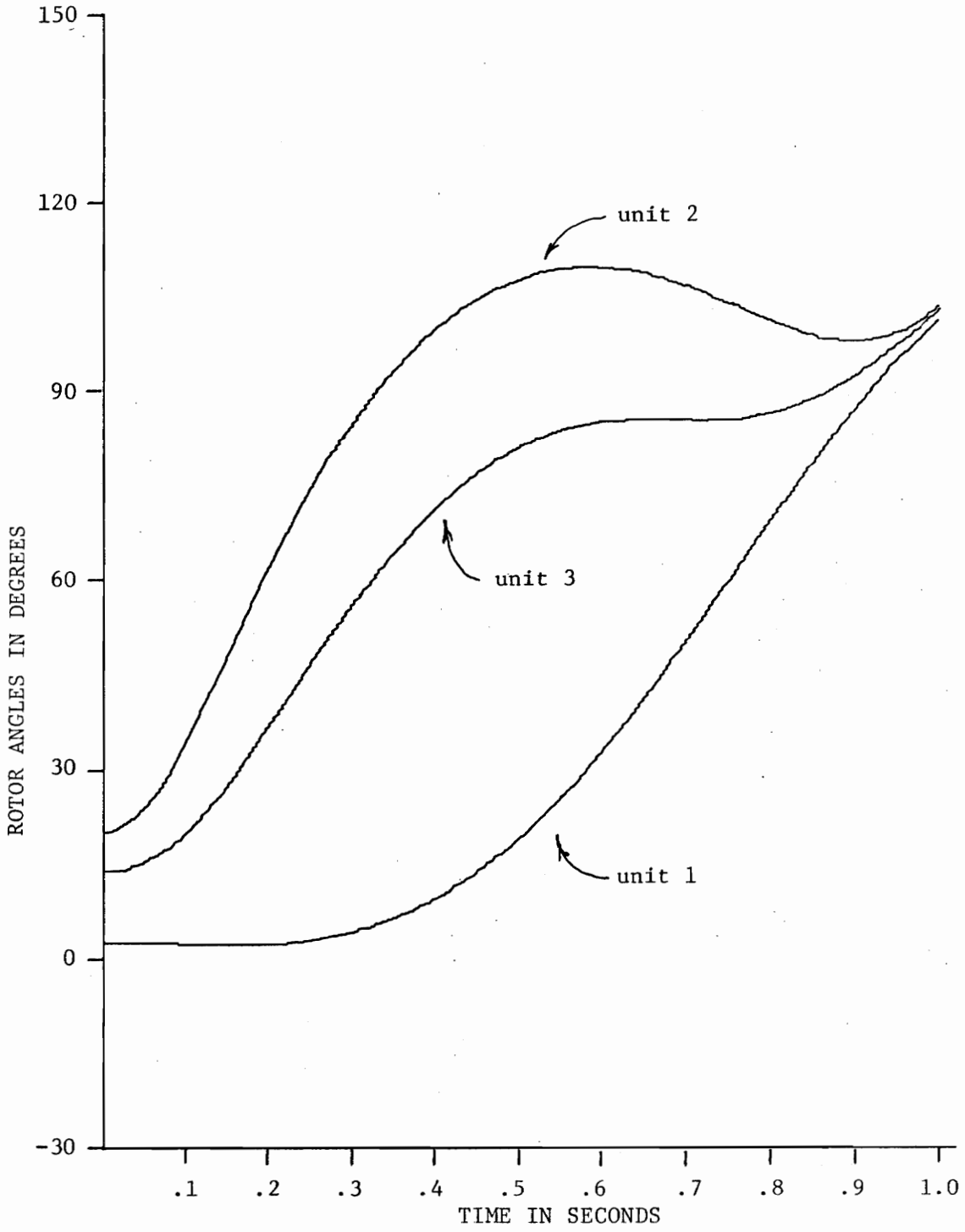

Fig. 3.3.5 Swing Curves
Induction Motors and Constant Impedance Loads (H = 300.0)

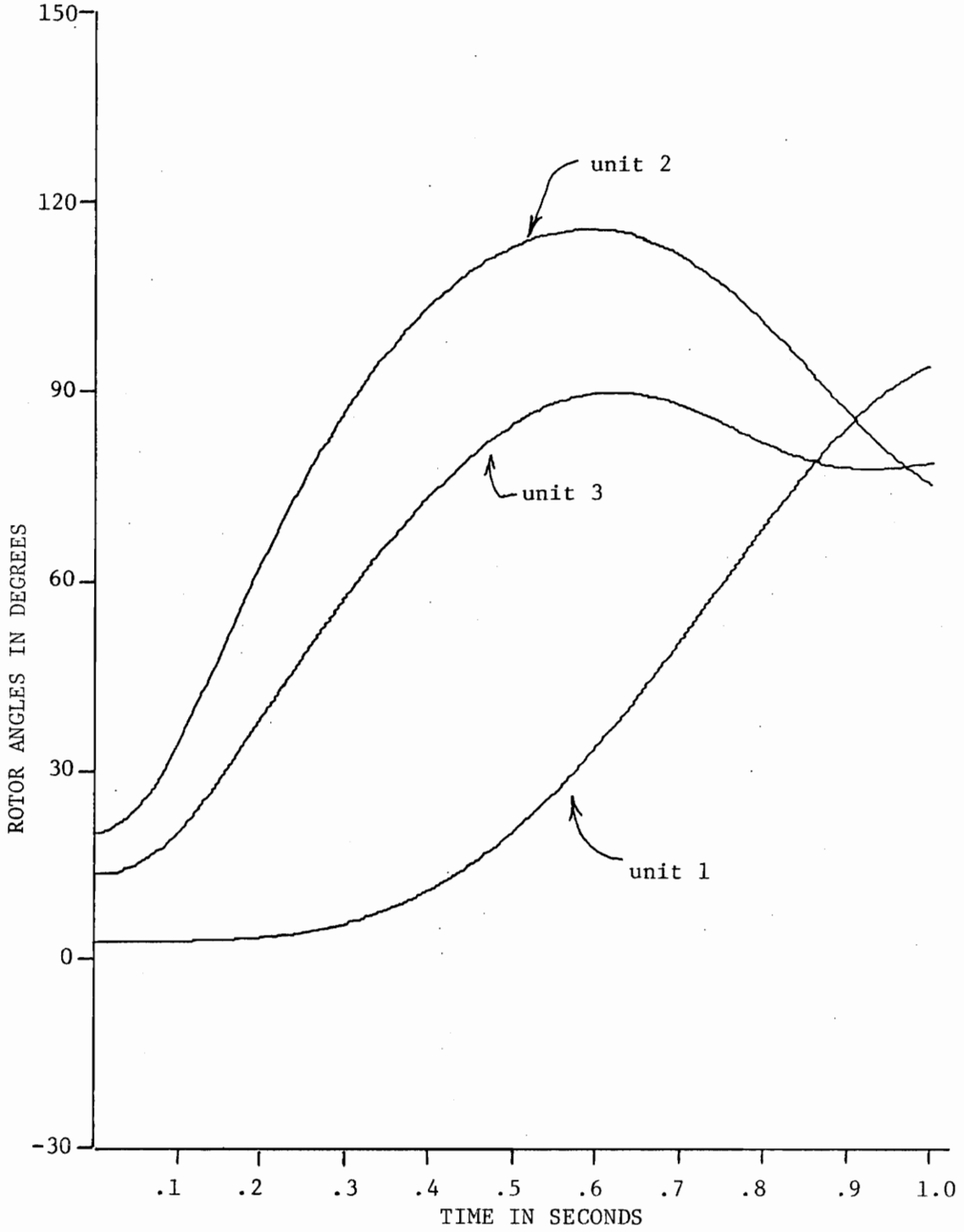

Fig. 3.3.6 Swing Curves
Mixed Dynamic Loading (H = 3.0)

Fig. (3.3.3) represents the behavior of the synchronous generators when the conglomerate induction motor is very "light", that is, H = 0.03 MW-s. This figure shows a marked improvement in generator swing over the most conservative classical load model, constant impedance.

Fig. (3.3.4) shows that, as the machine which represents the many small induction machines gets heavier (H = 3.0), the improvement over constant impedance decreases. This improvement, however, is nevertheless significant.

As the inertia constant of the induction machine gets very large (H = 300.0), the machine tends to behave more like a constant impedance load, as borne out by Fig. (3.3.5). This is due to the fact that the emf $\bar{E}'$ changes very slowly when the terminal conditions are changed. Even this very large inertia constant, however, produces results which tend to show that the constant impedance load is too conservative.

The last graph in this series (Fig. 3.3.6) shows the effect of mixed loading on the stability of the system. The load types included constant impedance, induction motors (H = 3.0), and some polynomial-fit loads (Table 3.2.4). These results represent the most accurate method of modeling loads. The curve, however, resembles very much the swing curve obtained by assuming all non-induction motor loads (H = 3.0) to be constant impedance (Fig. 3.3.4). Some conclusions will be drawn from this in the next chapter.

3.4 Load Bus Voltage Curves

Half of the research conducted herein has been aimed at modeling the loads as a function of voltage, not voltage independent as are the

classical load types. If the voltages of the load buses do not change appreciably, however, no justification exists for modeling a load as anything but voltage independent.

Fig. (3.4.1) through Fig. (3.4.6) represent the load bus voltage conditions associated with Fig. (3.3.1) through Fig. (3.3.6), respectively. In all cases the voltage swing at the load buses is considerable, up to a 0.8 p.u. voltage dip.

Fig. (3.4.1) and Fig. (3.4.2) represent a condition where the loads are inertialess, namely constant impedance and constant current. The bus voltages at these types of load buses change instantaneously with the onset and subsequent clearing of a fault.

In contrast to the first two figures in the section, Fig. (3.4.3) to Fig. (3.4.6) depict a smoother voltage transition at buses serving dynamic loads. The back-emf of the induction machines tends to slow down the voltage response to the fault. As one would expect, the voltages of the buses serving high-inertia machines swings more slowly than the corresponding voltages at buses serving low-inertia machines. The glitch in Fig. (3.4.6) is due to an undervoltage relay on the air conditioners closing upon fault clearance.

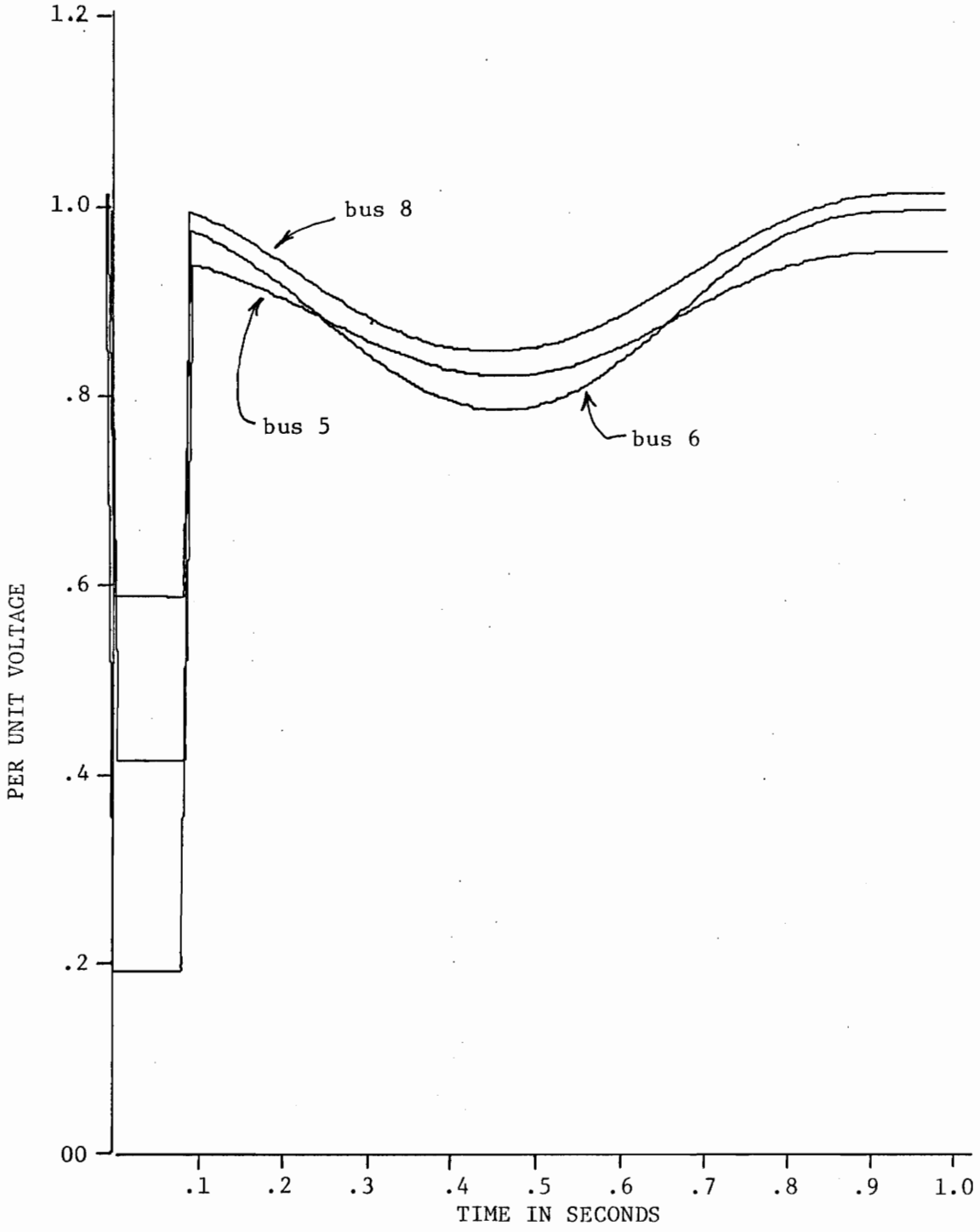

Fig. 3.4.1 Load Bus Voltage Curves
Constant Impedance Loads

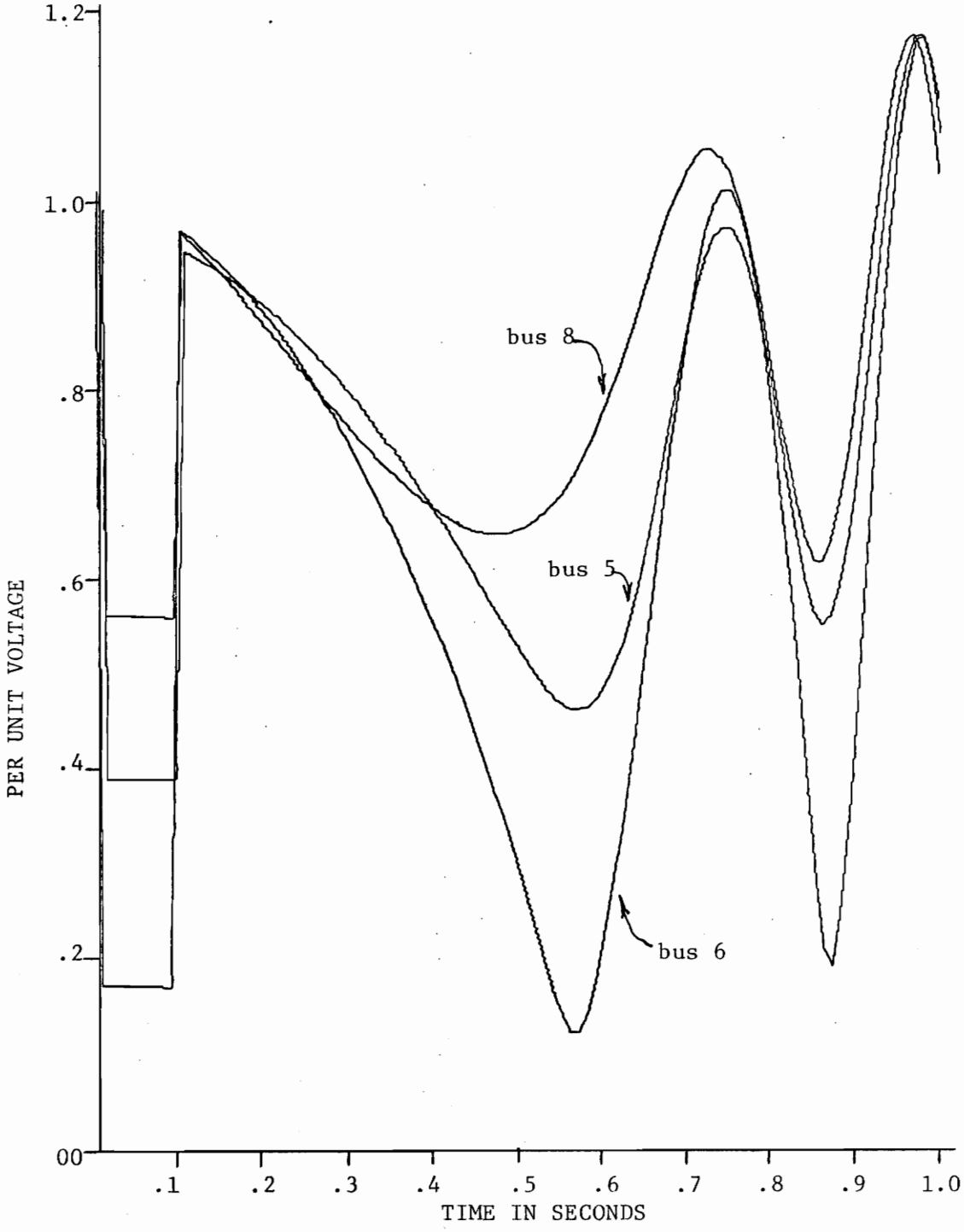

Fig. 3.4.2 Load Bus Voltage Curves
Constant Current Loads

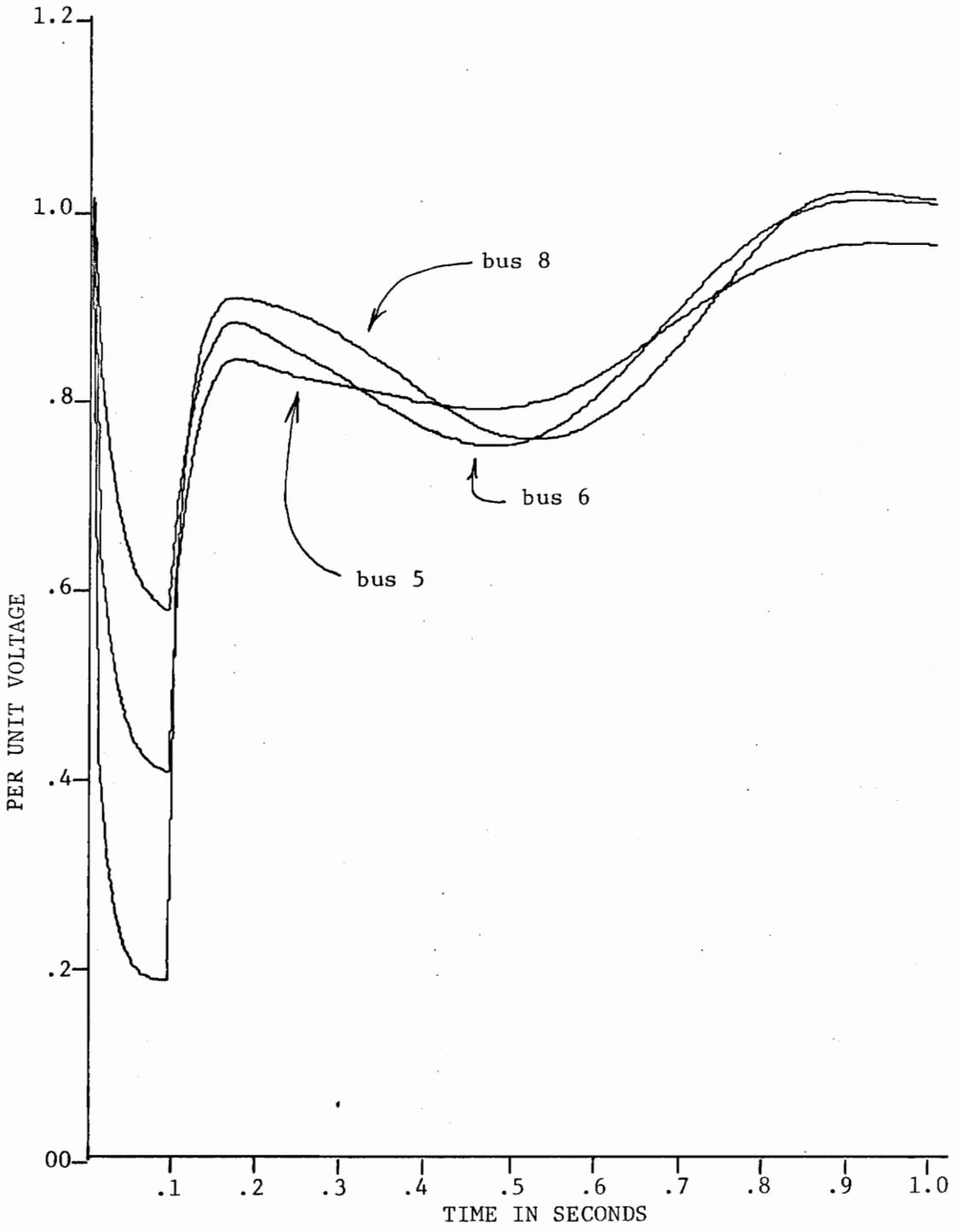

Fig. 3.4.3 Load Bus Voltage Curves
Induction Motors and Constant Impedance Loads (H = 0.03)

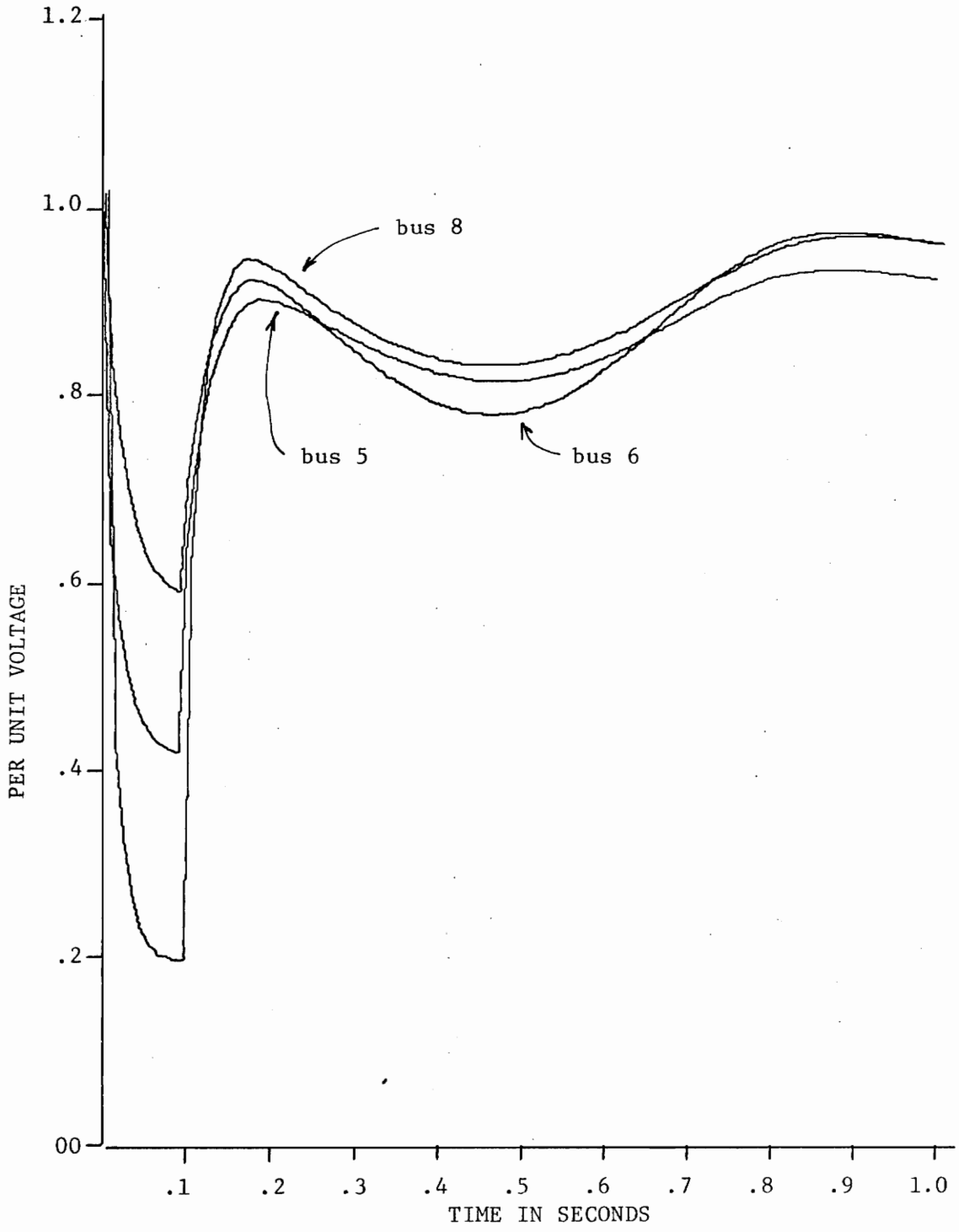

Fig. 3.4.4 Load Bus Voltage Curves
Induction Motors and Constant Impedance Loads (H = 3.0)

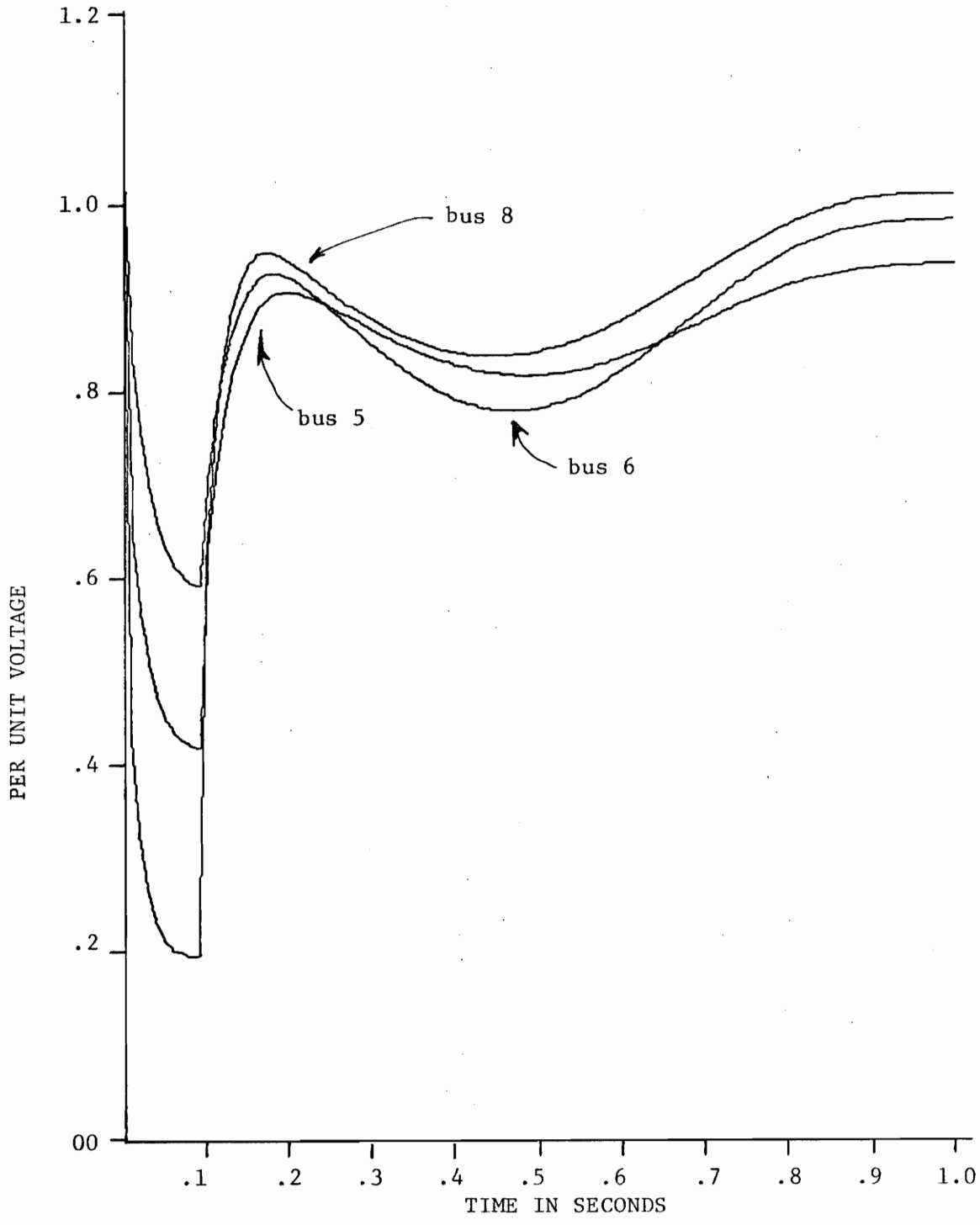

Fig. 3.4.5 Load Bus Voltage Curves
Induction Motors and Constant Impedance Loads (H = 300.0)

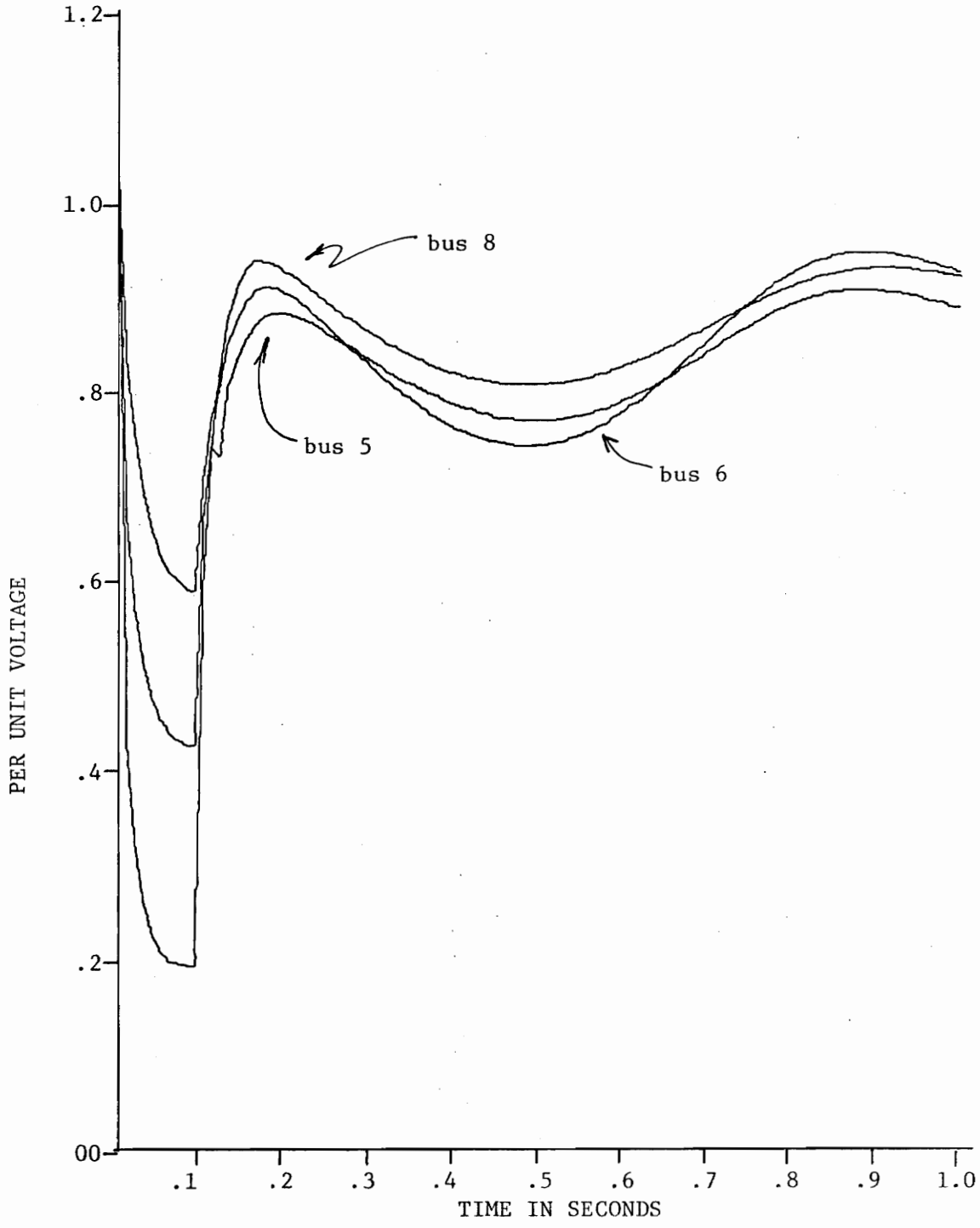

Fig. 3.4.6 Load Bus Voltage Curves
Mixed Dynamic Loading (H = 3.0)

4.0 CONCLUSIONS

In the previous chapter, the results of studying the effects of different load models on the swing curves of the generators were presented. Several trends are evident in examining these results.

In all the studies, the dynamic load model shows the constant impedance model to be too pessimistic. Even the extreme case when the inertia constant of the machine is very large (H = 300.0), dynamic load modeling shows systems to be overdesigned when the constant impedance load model is used.

The constant-MVA load model was not used in any of these studies since voltage convergence could not be achieved when the system was faulted. Since loads do not behave in this fashion during major system disturbances, the matter was not pursued any further.

When the loads were modeled as constant prefault current, the system became unstable very quickly. This represents a situation where the system is being overdesigned to a greater extent than by assuming all loads to be constant impedance.

One of the most important conclusions, however, is that modeling loads as polynomials in $|V|$ does not seem to make any appreciable difference in the final outcome when the bulk of the load (at least 50%) consists of induction motors. This may not be the case if the load consists mostly of fluorescent lighting, as may be the case in a heavily commercialized area. A utility serving primarily an industrial load or any type of load consisting of a large number of induction motors should not attempt to model the balance of the loads as polynomials in $|V|$.

This study, then, has shown that most electric power systems are too conservatively designed. This overdesign costs both the customer and the utility money that could be better spent elsewhere. In the days when systems were small and the capital involved was small, the "safe" approach was indeed feasible. But now, when an increasing number of utilities are being interconnected and the megawatt output of the plants gets larger and larger, a more realistic model for the loads must be used to ascertain the true behavior of the system during a major disturbance.

DYNAMIC LOAD MODELING IN POWER SYSTEM ANALYSIS

by

Joseph Roger Gracia

(ABSTRACT)

The objective of this thesis is to examine the effect of dynamic induction machine modeling and polynomial static load modeling on the stability of electric power systems and to compare the results with those obtained using constant impedance or constant current load models.

A least-squares curve fit algorithm is developed and used in modeling static and quasi-static loads as a function of the bus voltage.

A dynamic model for the induction machine which accounts for rotor electrical and mechanical transients is incorporated into the solution algorithm.

A test system is analyzed under a variety of loading conditions. The effect of the induction motor load inertia constants on the system stability are also examined. Plots of load bus voltages during the transient stability period are included.